Chemo-probe into the mantle origin of the NW Anatolia Eocene to Miocene volcanic rocks: implications for the role of, crustal accretion, subduction, slab roll-back and slab break-off processes in genesis of post-collisional magmatism

E. Yalçın Ersoy* [(1)], Martin R. Palmer[(2)], Ş. Can Genç[(3)], Dejan Prelević[(4,5)], Cüneyt Akal[(1)], İbrahim Uysal[(6)]

[(1)] Dokuz Eylül University, Department. of Geological Engineering, TR-35160, İzmir, Turkey

[(2)] School of Ocean and Earth Science, University of Southampton, National Oceanography Centre, European Way, Southampton SO14 3ZH, UK

[(3)] İstanbul Technical University, Department. of Geological Engineering, TR-34469 İstanbul, Turkey

[(4)] Institute for Geosciences, Johannes Gutenberg University, 55099 Mainz, Germany

[(5)] Faculty of Mining and Geology, University of Belgrade, Serbia

[(6)] Karadeniz Technical University, Department. of Geological Engineering TR-61080 Trabzon, Turkey

[(*)] **Corresponding author**:

Dr. E. Yalçın Ersoy
e-mail: yalcin.ersoy@deu.edu.tr
Tel: +90 (232) 301 73 46

Abstract

Post-collisional Paleogene magmatic activity in NW Anatolia produced widespread volcanism across the region. In the Biga Peninsula, in the west, medium-K calc-alkaline to ultra-K rocks with an orogenic geochemical signature were emplaced at ~43-15 Ma (*Biga orogenic volcanic rocks*; BOVR). Volcanic activity in the Central Sakarya region, to the east, is mainly restricted to ~53-38 Ma, but also continued during the Early Miocene with small basaltic extrusives (*Sakarya orogenic volcanic rocks*; SOVR). This study presents a new set of geochemical data (whole rock major and trace elements and Sr-Nd-Pb isotopic compositions), obtained from the Paleogene calc-alkaline volcanic rocks from these two regions. While there is considerable overlap in the emplacement time of volcanism in the two areas, the post-collisional volcanic rocks of these two regions differ in terms of their geochemical compositions: (1) the BOVR show an age-dependent increase in K and other large-ion lithophile elements (LILE), coupled with an increase in radiogenic Sr and Pb compositions from the Eocene to Miocene; whereas (2) the SOVR are characterized by more sodic compositions with lower K and less radiogenic Sr contents with respect to the BOVR, which were unchanged in Eocene and Miocene. We conclude that these geochemical features were principally related to the distinct modes of subduction-related mantle enrichment processes. We suggest that the Eocene to Miocene progressive enrichment in the BOVR mantle was related to successive subduction of oceanic and crustal materials in the western Aegean, while the SOVR mantle was dominantly enriched during the pre-collisional events. Magma generation in the western region was related to subduction roll-back processes associated with post-collisional extension. In the east, thermal perturbation of the mantle in response to asthenospheric upwelling due to slab break-off process was responsible for the magma generation. The time-dependent increase of K (and other LILE and radiogenic Sr) in the Cenozoic orogenic lavas from the Rhodope to Biga region emphasizes the importance of

crustal imbrication and subduction in the genesis of orogenic K-rich lavas of the Alpine-Himalayan orogenic belt.

Keywords: Aegean volcanism, subduction, mantle metasomatism, slab roll-back, slab break-off

1. Introduction

The north Aegean region has been shaped by: (a) northward subduction of Tethyan oceanic branches (e.g., the Intra-Pontide, Vardar and İzmir-Ankara Oceans) beneath Eurasia, (b) collision and accretion of continental blocks along the Eurasian margin, (c) roll-back and/or break-off of the subducted slabs, and (d) syn- to post-orogenic extensional deformation following the accretion processes, as a part of the Alpine-Himalayan orogenic system (Şengör and Yılmaz, 1981; Burg et al., 1996; Dinter, 1998; Ricou et al., 1998; Lips et al., 2000; Okay et al., 2001; Robertson and Ustaömer, 2004; van Hinsbergen et al., 2005; Bonev et al., 2006; Jolivet and Brun, 2010; Brun and Sokoutis, 2010; Gülmez et al., 2012, 2016; Akbayram et al., 2013; Ersoy and Palmer, 2013; Pourteau et al., 2016). Following Early Cretaceous collision and suturing along the Intra-Pontide Zone in NW Turkey (Akbayram et al., 2013), the Late Cretaceous northward subduction of the Vardar Ocean to the west and the İzmir-Ankara Ocean to the east resulted in development of the Srednogorie and Pontide arc magmatism along the southern Eurasian margin between ~95 to 68 Ma (von Quadt et al., 2005; Marchev et al., 2009; Georgiev et al., 2012; Yılmaz-Şahin et al., 2012) (Fig. 1). This was closely followed by suturing of micro-continents along the Vardar and İzmir-Ankara zones in the north Aegean-Anatolia region during the latest Cretaceous to Early Paleocene (Okay et al., 2001).

The northern Aegean to western Anatolia region had undergone extensive magmatic activity by the Eocene (Fig. 1). This magmatism is post-collisional with respect to the continental amalgamation along the Vardar and İzmir-Ankara suture zone, and lies in a back-arc position with respect to the present-day subduction front along Crete. An extensive suite of low- to high-K calc-alkaline, shoshonitic and ultrapotassic volcanic rocks was emplaced synchronously in Rhodope, the Thrace Basin and the Biga Peninsula at ~43 to 15 Ma. These rocks share largely similar geochemical characteristics revealing that they are orogenic in character (i.e., they originated from subduction-related metasomatic mantle domains) (see Christofides et al., 2004; Marchev et al., 2004; Ercan et al., 1995; 1998; Aldanmaz et al., 2000; Altunkaynak and Genç, 2008). To the east of NW Anatolia, in the Central Sakarya region, post-collisional volcanic activity began with Eocene activity that produced Na-alkaline basaltic to calc-alkaline rhyolitic orogenic volcanic rocks (~53 to 38 Ma; Kürkçüoğlu et al., 2008; Gülmez et al., 2012; Kasapoğlu et al., 2016). Local basaltic intrusions were also emplaced during the Miocene (~24 to 19 Ma; Kürkçüoğlu et al., 2008; Gülmez et al., 2012). Geochemical features of these Eocene (and local Miocene) volcanic rocks are interpreted as evidence for slab break-off following the arc-continent collision. Comparison of the geochemical features and relative timing of volcanic activity in the Central Sakarya region and the westerly-located Rhodope-Thrace-Biga region may thus yield a better understanding of the geodynamic evolution of the northern Aegean to NW Anatolian regions. With this aim, we have studied the detailed geochemical features and petrologic characteristics of the volcanic rocks in the Biga Peninsula (Fig. 2) and Central Sakarya region including the Lower Eocene Nallıhan volcanics (Fig. 3).

2. Regional Geology and Stratigraphy

The NW part of Anatolia (Fig. 1) contains Gondwana-derived continental fragments and intervening oceanic units that were accreted since at least Jurassic times (Şengör and Yılmaz, 1981; Okay et al., 1996). The boundary between the southerly-located Hellenides and Anatolide-Tauride Block, and the Rhodope-Pontide fragment occurs along the Vardar and İzmir-Ankara suture zones. The Rhodope-Pontide fragment is cut by the Upper Cretaceous (~95 to 68 Ma) Srednogorie arc volcanic and plutonic rocks (e.g., Georgiev et al., 2012). The Rhodope Massif was originally formed from an Alpine nappe package, and has subsequently been deformed by extensional tectonics since earliest Eocene, producing several core complexes and extensional metamorphic domes (Dinter, 1998; Kilias et al., 1999; Lips et al., 2000; Bonev et al., 2006; Brun and Sokoutis, 2010). This deformation was accompanied by extensive magmatism in the form of syn- to post-extensional granitoid plutons (~55 to 20 Ma), calc-alkaline to shoshonitic/ultrapotassic volcanic rocks (~43 to 26 Ma), and Na-alkaline OIB-like intra-plate basalts (~28 to 26 Ma) (Christofides et al., 2004; Marchev et al., 2004). The Rhodope and Strandja massifs also contain Paleogene – Neogene sedimentary rocks of the supra-detachment Thrace basin (Turgut et al. 1991; Siyako and Huvaz, 2007; Elmas, 2011; Kilias et al., 2013).

In the Biga Peninsula the basement units comprise metamorphic and non-metamorphic rocks of both the Rhodopean and Sakaryan affinities (e.g., Okay and Satır, 2000a; Beccaletto et al., 2007), which are separated by the ophiolitic Çetmi mélange, with eclogites having a metamorphic Rb-Sr age of ~100 Ma (Okay and Satır, 2000b) (Figs. 1 and 2). These rocks are cut and covered by Cenozoic magmatic and sedimentary units, with plutons from the Biga Peninsula having ages ranging from 48 to 37 Ma (Delaloye and Bingöl, 2000; Ustaömer et al., 2009; Altunkaynak et al., 2012a). Granitoid magmatism in the Biga Peninsula continued up to the Early Miocene with emplacement of extensive intrusions (Fig. 2; Delaloye and Bingöl, 2000; Karacık et al., 2008; Altunkaynak et al., 2012b; Aysal, 2015).

The Cenozoic volcanic units of Biga Peninsula are composed of; (1) Middle-Upper Eocene (~43 to 36 Ma) Balıklıçeşme volcanics, (2) Oligocene (~34 to 25 Ma) Kirazlı volcanics, (3) Upper Oligocene (28 to 23 Ma) Hallaçlar volcanics, (4) Lower-Middle Miocene Ezine-Ayvacık and Dedetepe volcanics, and (5) Upper Miocene (11.0 to 8.3 Ma) Taştepe basalts (see Supplementary Material 1 for the age data) (Ercan et al., 1995; 1998; Aldanmaz et al., 2000; Altunkaynak and Genç, 2008; Akal, 2013 and our unpublished data). Except for the Upper Miocene Taştepe basalts, which have distinctly Na-alkaline intra-plate composition, all the Eocene to Middle Miocene volcanic rock groups are orogenic in character; i.e., they are characterized by calcalkaline to ultrapotassic compositions with high LILE/HFSE ratios, high $^{87}Sr/^{86}Sr$ and low $^{143}Nd/^{144}Nd$ isotopic compositions indicating derivation from subduction-related enriched mantle domains. Compiled radiometric age data indicate that orogenic volcanic activity in the Biga Peninsula commenced at ~43 Ma and continued up to ~15 Ma, without any important interruption. These rocks are referred to as the Biga orogenic volcanic rocks (BOVR) in the following sections.

In the Central Sakarya region, the basement is made up of: (1) metamorphic and non-metamorphic rocks of the İstanbul and Sakarya Zones, which were juxtaposed during the Early Cretaceous, (2) ophiolite and ophiolitic mélange rocks of the İzmir-Ankara zone in the south of the region, which were underthrust by (3) the high-pressure schist and marble of the Tavşanlı Zone caused by northward migration of the Anatolide-Tauride Block (Fig. 3). The Upper Jurassic – Lower Cretaceous sedimentary cover of the Sakarya Zone is overlain by the Upper Cretaceous flysch-type sediments (Saner, 1980; Özcan et al., 2012), which pass southward into Paleocene reef limestones. The section is continued upward with the Kızılçay Group in the south (around Nallıhan) that contains the Nallıhan volcanics (~52–47 Ma) (Kasapoğlu et al., 2016). The correlative unit of the Kızılçay Group is the Çaycuma Formation in the north, which contains the basaltic to rhyolitic Eocene Kızderbent volcanics that yield ~53 to 38 Ma K-Ar and Ar-Ar radiometric ages (see Supplementary Material 1 for the age data) (Genç and Yılmaz, 1997; Kürkçüoğlu et al., 2008; Gülmez et al., 2012). There are also local Miocene basaltic extrusions emplaced between the Armutlu Peninsula and Almacık Mountains in this region (Fig. 3). In this study, the Eocene Kızderbent volcanics, Eocene Nallıhan volcanics and the local Miocene basaltic extrusives (Fig. 3) are referred to as the Sakarya Orogenic Volcanic Rocks (SOVR).

3. Analytical Methods

Here, we present a new dataset of geochemical analyses (whole-rock major and trace elements, Sr, Nd and Pb isotopes) from several volcanic units of the Biga and Sakarya orogenic volcanic rocks. In the Biga Peninsula we collected 65 samples from the Balıklıçeşme, Kirazlı, Hallaçlar and Dedetepe units. The petrographic and geochemical details of the Miocene Ezine-Ayvacık volcanics of the BOVR can be found in Genç (1998), Aldanmaz et al. (2000) and Akal (2013). We collected 22 samples from the Kızderbent volcanics in the Central Sakarya region. The geochemical details of the Eocene Nallıhan volcanics of the SOVR can be found in (Kasapoğlu et al., 2016). In addition, two high-pressure metamorphic rocks of the Tavşanlı Zone were sampled. All samples were powdered for whole-rock geochemical analyses by removing the altered surfaces and powdering in a tungsten carbide shatter box at Dokuz Eylül University.

3.1. Whole Rock Elemental Analyses

Element abundances of 89 samples were determined by inductively coupled plasma-atomic emission spectrometry (ICP-AES) (major elements) and ICP-MS (trace elements) in the ACME Laboratory, Canada, following lithium-borate fusion and dilute nitric acid digestion of a 0.1 g sample. Loss on ignition (LOI) was determined as the weight difference after ignition at 1000°C. Results of major and trace element analyses of the volcanic units in the study area are given in Supplementary Material 2.

3.2. Whole-Rock Sr-Nd-Pb Isotope Analyses

Analyses of Sr and Nd isotope ratios on 29 samples were carried out at the Central laboratory of the Middle East Technical University (METU, Ankara, Turkey), using procedures similar to those of Romer et al. (2001). ^{87}Sr/^{86}Sr data were normalized to ^{86}Sr/^{88}Sr of 0.1194. During the course of the study, Sr standard NIST SRM 987 was measured as 0.710247±10 (n=3). ^{143}Nd/^{144}Nd data were normalized to ^{146}Nd/^{144}Nd of 0.7219. Measurement of the La Jolla Nd standard gave a value of 0.511846±5 (n=3). The results are given in Table 1.

Pb isotope ratios were carried out on 18 samples at the University of Southampton (UK) using methods described in Ishizuka et al. (2007). Pb isotope analyses were conducted on a VG Sector 54 thermal ionization mass spectrometer and MC-ICPMS (Neptune) at Southampton. Both techniques used the double spike technique to correct instrumental bias (Ishizuka et al., 2007). Pb standard NBS 981 gave results of, 16.9404±32 (2SD) for ^{206}Pb/^{204}Pb, 15.4982±30 for ^{207}Pb/^{204}Pb and 36.7225±85 for ^{208}Pb/^{204}Pb for TIMS and 16.9403±27 for ^{206}Pb/^{204}Pb, 15.4973±21 for ^{207}Pb/^{204}Pb and 36.7169±66 for ^{208}Pb/^{204}Pb for MC-ICP-MS. The results are given in Table 2.

4. Results

4.1. Field Relations and Petrography

BOVR

The Eocene to Middle Miocene orogenic volcanic rocks of the Biga Peninsula comprise a large spectrum of petrographic compositions (basalt to rhyolite) and depositional modes (sub-marine ignimbrites, lava flows, widespread pyroclastic fall and flow deposits, dome and dike complexes) (Ercan et al., 1995, 1998; Genç, 1998; Aldanmaz et al., 2000; Yılmaz et al., 2001; Dönmez et al., 2005; Altunkaynak and Genç, 2008; Genç et al., 2012; Chakrabarti et al., 2012; Akal, 2013).

The Late Eocene Balıklıçeşme volcanics in the Biga Peninsula include basaltic to dacitic volcanic rocks. The widespread basaltic lava flows (Şahinli member) of this unit include large clinopyroxene phenocrysts with sizes up to 5 mm (Fig. 4a). The dacitic rocks located to the north of the region (Beyçayırı member) contain extensive amphibole and biotite in addition to plagioclase phenocrysts, which are embedded in a glassy matrix (Fig. 4b). The Kirazlı volcanics comprise more felsic associations of andesite, dacite, rhyolite and scarce basaltic rocks, relative to the Balıklıçeşme volcanics. They form widespread pyroclastic rocks with limited andesitic and dacitic lava flows, which are cut by andesitic to rhyolitic domes and dikes. The rhyolites typically comprise biotite, quartz, sanidine and plagioclase phenocrysts within volcanic glass (Fig. 4c). The Hallaçlar and Dedetepe volcanics are also composed of andesitic to rhyolitic compositions, with variable amounts of plagioclase, clinopyroxene, amphibole, biotite, quartz and sanidine. Opaque minerals are also seen in all samples. The Ezine-Ayvacık volcanics are mainly composed of andesitic to rhyolitic rocks with petrographic features of similar to those of the Dedetepe volcanics (see Genç, 1998; Aldanmaz et al., 2000 and Genç et al., 2012 for details). In addition to the felsic products, the leucite-bearing ultrapotassic dikes of ~21 Ma emplaced coeval with the Miocene Kestanbol granitoid (Akal, 2013). Finally, the Late Miocene Taştepe volcanics, with anorogenic geochemical signatures, are composed of several basaltic lava flows (see Aldanmaz et al., 2006 for details).

Kızderbent volcanics of the SOVR

The Eocene Kızderbent Volcanics include basaltic to andesitic syn-sedimentary lava flows and associated pyroclastic rocks and mafic dikes which are particularly prominent in the west of the region. The upper part of the section is marked by a transition from mainly pyroclastic to effusive activity, ending with olivine basalts (Genç and Yılmaz, 1997; Gülmez et al., 2012). Genç (2001) also reported the presence of metamorphic xenoliths in the andesitic rocks. The basaltic rocks include large clinopyroxene phenocryst (up to 3-5 mm) and subordinate altered olivine and plagioclase laths (Fig. 4d) but most of the samples are composed of euhedral plagioclase and lesser amounts of clinopyroxene phenocrysts embedded in a matrix of plagioclase laths and volcanic glass.

4.2. Whole-Rock Major and Trace Element Characteristics

The LOI values of the analyzed samples reach up to ~6% (Appendix 1), reflecting the fact that many of the magmatic rocks of the Biga Peninsula are variably affected by weathering or secondary alteration processes. We have therefore tested whether or not the element abundances of the rocks reflect their primary characteristics by applying the Chemical Index of Alteration (CIA; Nesbitt and Young, 1982) and the MFW plot of Ohta and Arai (2007). The CIA values of some of the dacitic-rhyolitic samples of the BOVR lie between 50 to 65, and reveal that these samples are slightly altered (Fig. 5a). Samples B-21, B-26 and C-20 also show alteration trends on the MFW plot of Ohta and Arai (2007) (Fig. 5b), but all the other samples lie on the primary magmatic trend on the MFW plot and have CIA values that are generally < 50. Overall, these alteration indices, together with the petrographic observations, suggest that the whole rock geochemical data can be used with confidence in the following discussion.

The geochemical data from this and previously published studies reveal that the BOVR are composed mainly of calc-alkaline basaltic to dacitic rocks with SiO_2 contents of ~45-70 (wt.%) and MgO contents of <9 (wt.%) (Figs. 6a and 6b). There are also rhyolitic samples with SiO_2 contents up to 75% (wt.%). In addition, leucite-bearing Miocene dikes have shoshonitic to ultrapotassic affinity (Akal, 2013). The K_2O contents of the calc-alkaline basaltic to dacitic rocks show an increase from the Middle-Late Eocene (Balıklıçeşme volcanics), through the Oligocene (Kirazlı and Hallaçlar volcanics) and eventually to the Miocene volcanics (Ezine-Ayvacık volcanics) (Fig. 6c). This temporal evolution is also apparent on the K_2O vs Na_2O plot (Fig. 6d) in which the Middle-Late Eocene Balıklıçeşme volcanics show a sodic to transitional affinity, while the Oligocene and younger lavas plot in the transitional to potassic (even ultrapotassic) fields.

The Lower-Middle Eocene Kızderbent volcanics (and the local Miocene basaltic extrusives) of the SOVR in the Central Sakarya region also comprise sub-alkaline basalt to andesite compositions, but are characterized by lower K_2O contents than the BOVR (Fig. 6c), and they form low- (tholeiitic) to medium-K calc-alkaline series with mainly sodic affinity (Fig. 6d). Most of the samples of the BOVR and Kızderbent volcanics have mainly silica-saturated to oversaturated compositions, with relatively few samples of silica-undersaturated basalts (normative nepheline <4%) (Fig. 6e). The leucite-bearing Miocene ultrapotassic dikes have distinctly higher normative nepheline contents (up to 17.5%; Akal, 2013). The Late Miocene Taştepe volcanics of the Biga Peninsula (and some samples from the Nallıhan volcanics of the SOVR) are characterized by strongly silica under-saturated, Na-alkaline basalts (see Aldanmaz et al., 2006; Kasapoğlu et al., 2016).

The BOVR and the Kızderbent volcanics of the SOVR show decreasing abundances of MgO, Fe_2O_3, CaO and TiO_2 with respect to increasing silica contents (Fig. 7). The Nallıhan volcanics of the SOVR are not included on these plots, because they have distinct geochemical features (Kasapoğlu et al., 2016). The Al_2O_3 and Na_2O contents show an increasing trend with silica for the basaltic to andesitic rocks, but a decrease or constant values, respectively in the andesitic to rhyolitic samples. For a given silica content, the Kızderbent volcanics have higher TiO_2 and Na_2O contents compared to the BOVR. The Ni, Cr and V contents all decrease from the basalts to rhyolites (not shown), but most of the other elements show more complex relationships with silica (Fig. 8). An important feature in Figure 8 is that the samples of the BOVR show silica- and time-dependent inter-element variations. For example, the Large Ion Lithophile Elements (LILE) (e.g., Ba and Sr) and light rare earth elements (LREE) (e.g., Ce) contents increase from the Eocene to the Middle Miocene, with the Kızderbent volcanics having the lowest concentrations of these elements. The Kızderbent volcanics also have relatively high concentrations of Zr, Y, and Yb. The Ce/Yb (and La/Yb) ratios of the BOVR units increase with both silica and decreasing ages. These age-dependent relationships are illustrated on Fig. 9.

On Normal-Mid Ocean Ridge Basalts (N-MORB)-normalized trace element plots (Fig. 10), both the BOVR and Kızderbent volcanics are characterized by enriched LILE and LREE abundances and relative depletions in high field strength elements (HFSE; Nb, Ta, Ti). The Middle-Late Eocene and Oligocene rocks of the BOVR (the Balıklıçeşme and Kirazlı volcanics) are also characterized by slight LILE enrichments compared to the Kızderbent volcanics of the SOVR (Figs. 10b and 10c). The trace element abundances and patterns of the Upper Oligocene samples of the BOVR (the Hallaçlar volcanics) more closely resemble those of the younger Miocene rocks in the region (the Dedetepe and Ezine-Ayvacık volcanics), and are more enriched than the older rock units (Figs. 10d and 10e). In Figure 10f the most primitive samples (lowest SiO_2 and highest MgO contents) from the BOVR and Kızderbent volcanics are also compared, with the Late Miocene Na-alkaline Taştepe basalts with no HFSE anomalies, and the Eocene Nallıhan volcanics of the SOVR showing more weakly developed HFSE anomalies.

4.3. Whole-Rock Sr-Nd-Pb Isotope Compositions

The initial $^{87}Sr/^{86}Sr$ and $^{143}Nd/^{144}Nd$ isotopic ratios of the SOVR Kızderbent volcanics (this study and previously published data) are in the range of 0.70397-70619 and 0.51254-0.51292, respectively. For the BOVR samples, these ratios vary in ranges 0.70462-0.70715 and 0.51243-0.51269, revealing that these rocks have slightly higher Sr and lower Nd ratios than the more easterly located Kızderbent volcanics (Fig. 11a). The Lower Miocene rocks of the BOVR, however, have much more enriched radiogenic Sr and unradiogenic Nd contents than the preceding Eocene-Oligocene rocks of the group. The increasing radiogenic Sr ratios, with decreasing ages of the studied rocks are also apparent on an $^{87}Sr/^{86}Sr_{(i)}$ vs SiO_2 plot (Fig. 11b), which shows that (with the exception of the Late Miocene Na-alkaline basalts) the Lower Eocene volcanic rocks are characterized by the lowest $^{87}Sr/^{86}Sr_{(i)}$, while the Miocene rocks have the highest ratios for a given silica content among the calc-alkaline suites. The calc-alkaline Kızderbent volcanic products also have the lowest $^{206}Pb/^{204}Pb_{(i)}$ and $^{208}Pb/^{204}Pb_{(i)}$ (Figs. 11c and 11d). All the BOVR and SOVR samples lie on a trend between MORB and Enriched Mantle-II (EM-II) end-members (Fig. 11d).

5. Discussion

All the studied volcanic samples have Ni <100 ppm and MgO < 8 (wt.%) contents, indicating that they do not represent primary melt compositions derived from mantle sources, hence the variable effects of crystal fractionation and possible crustal contamination (AFC) processes will be discussed first. Their mantle source characteristics and melting conditions will then be explored using abundances and ratios of specific elements and isotopes of the most primitive samples, which are least affected by AFC processes. The discussion above indicates that there are clear differences between the geochemical compositions and stratigraphic associations of the BOVR and SOVR areas. In addition, the rocks of the BOVR show time-dependent geochemical trends that may reflect the geodynamic evolution of the region.

5.1. Fractional Crystallization and Crustal Contamination Processes

The possible effects of fractional crystallization with or without crustal contamination (assimilation) (FC and AFC processes) on the genesis of the studied calc-alkaline volcanic rocks have already been reviewed (Genç and Yılmaz, 1997; Genç, 1998; Aldanmaz et al., 2000; Yılmaz et al., 2001; Altunkaynak and Genç, 2008; Kürkçüoğlu et al., 2008; Gülmez et al., 2012; Kasapoğlu et al., 2016), hence these processes will only be examined briefly here. Decreasing contents of MgO, Fe_2O_3, CaO, TiO_2, Ni, Cr, Sc and V with respect to increasing silica for the basaltic to andesitic rocks (SiO_2: ~45% to 60%) indicate that olivine, clinopyroxene, and Fe-Ti oxides are crystallized and removed from the evolving melts during FC processes (Figs. 7 and 8). Further decreases in these elemental abundances, together with decreasing trends for Al_2O_3, Na_2O and Sr, for the andesitic to rhyolitic rocks, are interpreted as evidence for subsequent FC of clinopyroxene, amphibole, plagioclase and Fe-Ti oxides. Evidence for these fractionation assemblages is also supported by petrographic observations of the presence of these minerals as suspended phenocrysts. For example, the presence of poikilitic pyroxenes with olivine and plagioclase inclusions in the Eocene basaltic lavas of the BOVR indicates that pyroxene crystallization was preceded by olivine and plagioclase crystallization (Fig. 4a).

Potential crustal contamination during crystal fractionation (AFC process) can be examined by using the Sr isotopic ratios of the basic to acid magmatic rocks in a co-magmatic suite. An increase in $^{87}Sr/^{86}Sr$ ratios from basic to more acid samples likely reflects contribution from the crustal rocks with high radiogenic Sr contents, and can be monitored on $^{87}Sr/^{86}Sr$ vs SiO_2 plot. Collectively, the volcanic groups considered here show a variable, but generally positive trend for $^{87}Sr/^{86}Sr$ vs SiO_2 (Fig. 11b), indicating that AFC processes played a role in the geochemical evolution of these rocks. The andesites of the Kızderbent volcanics also contain partly digested metamorphic xenoliths and garnet crystals (Genç, 2001), that are clear evidence of crustal assimilation and magma contamination. Genç (2001) also noted that the andesite-hosted garnets are compositionally similar to those within the xenoliths.

The complex history of crustal accretion in the region covered by this study has resulted in a wide range of basement types; hence it is difficult to numerically model AFC processes by using limited parameters. This complexity may also contribute to the wide range in $^{87}Sr/^{86}Sr$ ratios *within* each of the volcanic units for a given silica content. It should also be noted, however, that there is no clear correlation between the $^{87}Sr/^{86}Sr$ ratios and silica contents *between* different units illustrated in Figure 11b. Similar observations (not shown) can be drawn from the Nd and Pb isotopic ratios. Thus, we suggest that the differences in isotopic compositions between the different groups cannot be explained by AFC processes alone, but rather these differences also likely reflect some geochemical variation/differentiation in their mantle sources.

5.2. Mantle Source Characteristics and Melting Conditions

Mantle Background

The La/Yb vs La and Nb/Zr vs Nb systematics of the various BOVR and SOVR units are principally dependent on the nature of the mantle source and variable degrees of melting of that source (Figs. 12a and 12b). Hence, positive correlations on these plots can yield information concerning the source characteristics and melting conditions.

The Nb/Zr vs Nb relationships do not depend on subduction-related source enrichment and/or crustal contamination of the magmas, and potential mantle sources [primitive mantle (PM), depleted MORB mantle (DMM), enriched DMM (E-DMM) and depleted-DMM (D-DMM) compositions (Palme and O'Neil 2004; Workmann and Hart, 2005) describe a near-vertical chemical variation trend on Figure 12b. On this plot, the Kızderbent volcanics have lower Nb/Zr ratios for given Nb contents and are compatible with being derived from a more depleted mantle source (D-DMM) compared to the Biga calc-alkaline rock groups, which converge on a DMM composition (Fig. 12b).

The effects of subduction-related enrichment of the mantle sources will be discussed below, but it is important to note that the SOVR units (the Kızderbent and Nallıhan volcanics in the east) show more variable and generally higher Nb/La and Nb/Ba ratios than the BOVR (Figs. 12c and 12d). The Late Miocene Na-alkaline basaltic rocks of NW Anatolia, namely Taştepe volcanics, have relatively high Nb/La and Nb/Ba ratios that likely represent melts derived from mainly asthenospheric mantle sources ("*within plate*" fields on Figs. 12c and 12d) (Aldanmaz et al., 2006). Hence there appears to be a trend in Nb/La and Nb/Ba ratios from the Na-alkaline intra-plate basaltic field to the SOVR that is most obvious for the low silica samples. This trend may reflect the presence of a high Nb/La, possibly asthenospheric component in the origin of the SOVR in the east. In contrast, the BOVR show lower and more constant Nb/La and Nb/Ba ratios over a wide range of silica contents ("*subduction-related*" fields on Figs. 12c and 12d). This comparison suggests that the BOVR were derived from mantle lithosphere that had been highly enriched by subduction-related metasomatism (i.e., they have *orogenic* character), whereas the SOVR contain a greater asthenospheric mantle contribution.

Mantle Enrichment Processes

The MORB-normalized multi trace element spider patterns of the most primitive BOVR and SOVR samples are characterized by Nb and Ta negative anomalies with respect to neighboring LILE and LREE (Fig. 10f), and is also reflected in their low Nb/La and Nb/Ba ratios (Figs. 12c and 12d). These features are indicative of derivation from mantle sources which had been enriched by subduction zone components (Genç and Yılmaz, 1997; Aldanmaz et al., 2000; Yılmaz et al., 2001; Altunkaynak and Genç, 2008; Kürkçüoğlu et al., 2008; Gülmez et al., 2012). This interpretation is also supported by the Th/Yb vs Nb/Yb systematics (Pearce, 2008). On this plot (Fig. 13a), the Late Miocene Taştepe Na-alkaline basalts plot along the mantle array, whereas the BOVR and the Kızderbent volcanics plot parallel to and above the mantle array, indicating they were derived from mantle sources that had been enriched by addition of subduction zone components (SZC). It is also noteworthy that the mantle source of the Kızderbent volcanics appears to be more depleted (similar to DMM), and was more enriched by higher degrees of SZC, compared to the mantle source of Nallıhan volcanics of the SOVR (see also Kasapoğlu et al., 2016).

In addition to their different trace element abundances, the SOVR and the BOVR differ in their radiogenic isotope compositions, with the former having less radiogenic Sr and Pb isotope ratios (Fig. 11). There is also a time-dependent increase in the Sr isotopic ratios of the BOVR: (1) the Middle Eocene to Oligocene rocks of the BOVR have uniform and the lowest Sr isotopic ratios, while the Lower to Middle Miocene rocks of the BOVR with the Miocene volcanic rocks of NW Anatolia show the highest Sr ratios for a given silica composition (Fig. 11b). This age-dependent isotopic variation among these groups is also reflected in their K and other LIL element variations (Fig. 9). The consistency of these patterns, particularly for the most basic (primitive) samples of the rock groups, may thus reflect enrichment of their mantle sources by SZC with time.

The Ba/Zr vs Nb/Zr systematics of the most primitive samples are also considered in Figure 13b, because these ratios are nearly independent of fractional crystallization. The mantle array on this plot is marked by using D-DMM, DMM and E-DMM compositions, and describes a positive correlation for an enrichment trend. Partial melting of a mantle source will also result in a positive trend in Ba/Zr vs Nb/Zr ratios, as described by incremental melt compositions obtained using a dynamic melting equation (Zou, 1998) with a starting composition of D-DMM (Workmann and Hart, 2005) (Figure 13b). It is therefore apparent from the trend illustrated in Figure 13b that closed-system melting of a source lying on the mantle array cannot produce the data observed in the orogenic rock units, which are characterized by higher Ba/Zr ratios. Instead, the geochemical features of the studied rocks require a mantle source that is more enriched in Ba/Zr, which can most readily be supplied by subduction-related enrichment processes. It is also noteworthy that the BOVR require a more enriched source than the Kızderbent volcanics.

The Sm-Nd isotopic systematics of the studied rock groups can also be described in terms of their Depleted Mantle (DM) model ages (T_{DM} DePaolo, 1981). Two-stage DM model ages

(T_{DM2}) are frequently used for felsic rocks (Liew and McCulloch, 1985) because they give better insights into the crustal components in magmatic rocks derived from metasomatic mantle (Fig. 13c). The resultant T_{DM2} ages range from 300 to 800 Ma in the SOVR and 700 to 1500 Ma in the BOVR (Table 1). The latter group also shows age-dependent increases in T_{DM2} ages with the NW Anatolia Miocene volcanic rocks yielding the highest model ages. According to the T_{DM2} vs Nb/La systematics, the data from the Nallıhan volcanics lie on a trend between the Na-alkaline basalt field and the other rock groups, which again supports the presence of an asthenospheric component in their origin. On this plot the Kızderbent volcanics scatter between the trend lines from Na-alkaline basalt and MORB fields and evolve towards high T_{DM2} and low Nb/La values with time. The higher T_{DM2} ages of the BOVR are compatible with the higher amounts of crustal components in their mantle source regions.

In an effort to better understand the nature of the subduction zone component involved in the genesis of the studied rock groups, we analyzed whole-rock elemental and Sr-Nd isotopic compositions of two high-pressure (HP) metasedimentary rocks from the Tavşanlı Zone (Table 1). These HP rocks represent the portions of the Anatolide-Tauride Platform that were subducted to a depth of ~80 km in an intra-oceanic subduction system (i.e., early stages of collision; Okay et al., 2001; Pourteau et al., 2016 and references therein). These data were then used to calculate several subduction zone components: slab melt (SM1 and SM2) and slab fluid (SF1 and SF2) using the fluid and melt distribution coefficients of Johnson and Plank (1999) (Table 3). The resultant compositions were then used to contaminate (by simple mixing models) the possible depleted mantle compositions, with the results summarized on a $^{143}Nd/^{144}Nd_{(i)}$ vs Nb/La plot (Fig. 13d). The very limited effects of high-degree FC and AFC processes (with crystallization ratio of 90% and relative ratios of assimilated material to crystallized material of 0.2 and 0.5) are also modelled to show that the geochemical characteristics of the samples on this plot are not predominantly controlled by these secondary processes, and hence likely reflect the source enrichment processes. Because the Nb/Zr vs Nb systematics (which are independent of metasomatic enrichment processes) indicate that the original mantle composition requires a D-DMM source (Fig. 12b), the best results for the Kızderbent volcanics are obtained by adding ~1.0-2.5% SF2 to this mantle source, followed by high degree AFC processes. The compositions of the Middle Eocene – Oligocene rocks of the BOVR require a slightly higher contribution (~2.5-4.0%) from the SF2 component to the D-DMM or DMM source (which also followed by high degree AFC processes) to produce the other evolved magmas. The HP rocks of the Tavşanlı Zone are considered as a possible candidate responsible for metasomatism of the mantle beneath the Central Sakarya region because this unit tectonically underlies the Sakarya Zone in this region (Fig. 1). If similar material to the Tavşanlı Zone had also been subducted beneath the Rhodope-Biga region, this would imply that the rocks of the BOVR require an even greater contribution from subducted components. This interpretation is also consistent with the trends displayed in Figure 11d, which show that the BOVR require a greater contribution from EMII sources (i.e., a continental crust-like reservoir). As noted before, however, the Nallıhan volcanics of the SOVR require a more primitive, OIB-like mantle sources (E-DMM or more enriched sources like that of OIB) to be contaminated by subduction components.

__Partial Melting Processes__

The depth of mantle melting events can be constrained from the mineralogical composition of the mantle sources (e.g., spinel- or garnet- mineralogical association as shallow- or deep-mantle sources). Constraining the mantle source mineralogy responsible for formation of the primary melts can be accomplished by using Tb/Yb vs La/Yb ratios of the resultant volcanic rocks (e.g., Ellam, 1992). This mainly depends on fractionation of Tb/Yb ratios in the melts during the melting event, which is controlled by the bulk partition coefficient of the medium to heavy REE in the spinel and garnet-bearing source peridotites (Ellam, 1992). This approach also has the advantage that FC/AFC processes do not significantly affect these ratios. It is also noteworthy that these ratios can be influenced by the mineralogy of subducted material which metasomatized the original mantle source (i.e., the presence of garnet in the subducted materials) from which the fluid/melts were released during subduction (e.g., Avanzinelli et al., 2008).

On a Tb/Yb and La/Yb log-log plot (Fig. 14), the data from the Kızderbent volcanics of the SOVR define a parallel trend to the mantle array, indicating that garnet was absent in the mantle domain and in the (subducted) metasomatizing material. This observation is also consistent with the MORB-normalized spider plots of this group (Fig. 10a), where the most primitive samples are characterized by near flat patterns with $Tb/Yb_{(n)}$ ratios of ~1.2 – 1.6. However, the Tb/Yb and La/Yb ratios values of the BOVR increase from the Middle Eocene to Miocene samples (Fig. 9d). These variations can also be seen on the spider plots (Fig. 10b – 10d), where their $Tb/Yb_{(n)}$ ratios increase from ~1.0 – 1.5 to ~1.5 – 2.5, respectively. This time-dependent increase in Tb/Yb values of the BOVR may indicate that their mantle source (or the subducted materials) became garnet-bearing with time. Alternatively, this trend may mean that the depth of melt production increased over time and may thus be indicative of lithospheric thickening.

5.3. Geodynamic Implications

The subduction-related chemical signature in the mantle sources of the Eocene to Miocene SOVR and BOVR (i.e., their orogenic character) may result from mantle enrichment processes during a previous (Late Cretaceous) subduction event, or subduction concurrent with the period of volcanism. Alternatively, the geochemical trends may result from derivation from a previously enriched, much older lithospheric mantle source. Geochemical evaluation of the Eocene SOVR units located in the east of the study area (the Kızderbent volcanics of 53 to 38 Ma [Gülmez et al., 2012], and the Nallıhan volcanics of 52 to 47 Ma [Kasapoğlu et al., 2016]; Figure 1) imply that they all reflect some degree of subduction-induced enrichment in their sources, but that the Nallıhan volcanics, situated along the south of this region, are more strongly influenced by an asthenospheric sources. Although this asthenospheric source was also present to a lesser degree in the Kızderbent volcanics, this group originated mainly from a MORB-like mantle source. Overall, these geochemical features are interpreted to be the consequence of slab break-off processes following the Late Cretaceous-Paleocene collision of the Central Sakarya region in the east (see also Gülmez et al., 2012; Kasapoğlu et al., 2016). In this scenario, the metasomatic signature involved in the genesis of the SOVR was related to Late Cretaceous subduction of the northern Neo-Tethys beneath the Pontides, with the higher asthenospheric component in the Nallıhan volcanics with respect to the Kızderbent volcanics resulting from their closer location to the subduction hinge where the slab break-off occurred. In addition, because there is no clear compositional difference between the Lower Eocene Kızderbent volcanics and the Miocene basaltic extrusions in this region, this suggests that the mantle source beneath the region has remained largely unchanged through the Cenozoic.

Geochronology data reveal that post-collisional orogenic volcanism in the Biga Peninsula (BOVR) began ~43 Ma and continued up to ~15 Ma. While precise dating of the subduction-related metasomatism of their mantle source is not possible with available data, the geochemical data clearly demonstrate the presence of time-dependent elemental and isotopic variations among the BOVR. For example, the increasing radiogenic Sr isotope composition of the volcanics (e.g., Figs. 9 and 11b) and the increasing K (and other LILE) contents with decreasing age, suggests that the mantle source beneath the Biga Peninsula became progressively enriched by increased addition of crustal materials from the Eocene to the

Miocene. This may be explained by successive subduction, collision and crustal-accretion events in the western Aegean, including the Biga Peninsula (van Hinsbergen et al., 2005; Jolivet and Brun, 2010). Such a time-dependent geochemical variation in the Cenozoic orogenic lavas from the Rhodope to Biga region emphasizes the importance of crustal imbrication and subduction in the genesis of orogenic K-rich lavas seen across much of the Alpine-Himalayan orogenic belt (see also Ersoy and Palmer, 2013).

The magmatic activity producing the BOVR (and along the Rhodope region) was also likely related to extensional tectonics in response to roll-back of the subducted slab on which the crustal slivers was progressively accreted (Okay and Satır, 2000b; van Hinsbergen et al., 2005; Jolivet and Brun, 2010; Brun and Sokoutis, 2010; Ersoy and Palmer 2013; Ersoy et al., 2014). The crustal accretion model on a single subducting plate for this region is also supported by the increasing Tb/Yb ratios of the Biga calc-alkaline volcanic units, which may indicate lithospheric thickening by crustal imbrication and accretion.

The distinct geodynamic histories of the Biga Peninsula (and Rhodope region) and the Central Sakarya region, revealed by the Eocene to Miocene orogenic volcanic rocks, was also likely related to the behavior of the subducted Tethys slabs. While the subducting slab in the western side of the region (beneath the Rhodope to Biga region) was migrating south by accretion of the overlying continental blocks, and was giving rise to progressively more contaminated mantle sources, the subducting slab in the eastern side broke-off (beneath the Central Sakarya region). This distinct behavior of the subducting slabs in the west and in the east, following the Late Cretaceous collision was accommodated by a strike-slip movement along İzmir-Balıkesir Transfer zone (Figure 1; Ersoy and Palmer 2013).

6. Conclusions

Two regions in NW Anatolia, the Biga Peninsula in the west and the Central Sakarya region in the east, contain basaltic to rhyolitic volcanic rocks with ages of ~43 to 15 Ma and ~53 to 38 Ma, respectively. All these rock groups are post-collisional with respect to the Late Cretaceous – Paleocene closure of the northern Neotethys oceanic branches, but while both these areas contain volcanic and plutonic rocks with orogenic geochemical features, there are clear spatial and temporal geochemical differences between and within the two groups.

The E-W-trending orogenic rocks of the Central Sakarya region (SOVR) were emplaced mainly during the Early Eocene and, to a lesser extent, in the Early Miocene. The geochemical features of these rocks did not change significantly during this time, and reveal that their sources were affected by both asthenospheric (convecting) and lithospheric (MORB mantle) mantle sources, which were metasomatized by subducted sediments during Late Cretaceous Tethyan-ocean subduction. Extensive crustal assimilation coupled with fractional crystallization processes of the magma batches also occurred within the continental crust after primary melt formation.

The orogenic magmatic rocks of the Biga Peninsula (BOVR) were emplaced between the Middle Eocene to Middle Miocene, and do not show any clear asthenospheric signature in their genesis. Instead, they appear to be derived from a MORB-like mantle source which was initially enriched during the Late Cretaceous. Following this, the mantle source was progressively re-enriched by subduction of continental slivers during accretion processes on a southward migrating single subduction system. Successive addition of continent-derived materials in the mantle sources gave rise to progressive enrichment of K (and other LILE, radiogenic Sr, etc.) in the resultant magmas over this time.

Within the geodynamic history of the region, we suggest that the SOVR formed by asthenospheric upwelling and related thermal perturbation in response to the trench-parallel break-off of the subducted slab in the eastern side of the Neotethys following the continental collision. In contrast, the BOVR (possibly together with the orogenic volcanics in the Rhodope region) formed in an extensional tectonic regime associated with the southward roll-back of the subducted slab along western side of the Neotethys and accretion of the overlying crustal blocks. The distinct behavior of the subducted slabs in the west and the east of the region was accommodated by a transfer fault that has been in existence since Late Cretaceous, and is now present as the İzmir-Balıkesir Transfer Zone (Fig. 1). Time-dependent increase of K (and other LILE and radiogenic Sr) in the Cenozoic orogenic lavas from the Rhodope to Biga region emphasizes the importance of crustal imbrication and subduction in the genesis of orogenic K-rich lavas of the Alpine-Himalayan orogenic belt.

Acknowledgments

This work supported by the Scientific and Technological Research Council of Turkey (grant number: TUBITAK-CAYDAG-12Y128). Bülent Kasapoğlu, Okan Bektaş, Uğur Öven, Selen Özdemir and Zehra Soysal are thanked for their help during field studies and sample preparation processes. We wish to thank to Serhat Köksal (Middle East Technical University, Central Laboratory) who carried out the Sr and Nd isotopic measurements and to Agnes Michalik and Rex Taylor (Southampton University) for help with the Pb isotope measurements.

References

Adam, J., Green, T., 2006. Trace element partitioning between mica- and amphibole bearing garnet cpx–harzburgite and hydrous basanitic melt: 1. Experimental results and the investigation of controls on partitioning behavior. Contributions to Mineralogy and Petrology 152, 1–17.

Akal, C., 2013. Coeval Shoshonitic-Ultrapotassic Dyke Emplacements within the Kestanbol Pluton, Ezine – Biga Peninsula (NW Anatolia). Turkish Journal of Earth Sciences 22, 220–238.

Akbayram, K., Okay, A.I., Satır, M., 2013. Early Cretaceous closure of the Intra-Pontide Ocean in western Pontides (northwestern Turkey). Journal of Geodynamics 65, 38–55.

Aldanmaz, E., Köprübaşı, N., Gürer, Ö.F., Kaymakçı, N., Gourgaud, A., 2006. Geochemical constraints on the Cenozoic, OIB-type alkaline volcanic rocks of NW Turkey: Implications for mantle sources and melting processes. Lithos 86, 50–76.

Aldanmaz, E., Pearce, J.P., Thirwall, M.F., Mitchell, J.G., 2000. Petrogenetic evolution of late Cenozoic, post-collision volcanism in western Anatolia, Turkey. Journal of Volcanology and Geothermal Research 102, 67–95.

Altunkaynak, Ş., Dilek, Y., Genç, C.Ş., Sunal, G., Gertisser, R., Furnes, H., Foland, K.A., Yang, J., 2012b. Spatial, temporal and geochemical evolution of Oligo–Miocene granitoid magmatism in western Anatolia, Turkey. Gondwana Research 21, 961–986.

Altunkaynak, Ş., Genç, C.Ş., 2008. Petrogenesis and time-progressive evolution of the Cenozoic continental volcanism in the Biga Peninsula, NW Anatolia (Turkey). Lithos 102, 316–340.

Altunkaynak, Ş., Sunal, G., Aldanmaz, E., Genç, C.Ş., Dilek, Y., Furnes, H., Foland, K.A., Yang, J., Yıldız, M., 2012a. Eocene Granitic Magmatism in NW Anatolia (Turkey) revisited: New implications from comparative zircon SHRIMP U–Pb and ^{40}Ar–^{39}Ar geochronology and isotope geochemistry on magma genesis and emplacement. Lithos 155, 289–309.

Avanzinelli, R., Elliot, T., Tommasini, S., Conticelli, S., 2008. Constraints on the Genesis of Potassium-rich ItalianVolcanic Rocks from U/Th Disequilibrium. Journal of Petrology 49, 195–223.

Aysal, N., 2015. Mineral chemistry, crystallization conditions and geodynamic implications of the Oligo–Miocene granitoids in the Biga Peninsula, Northwest Turkey. Journal of Asian Earth Sciences 105, 68–84.

Beccaletto, L., Bonev, N., Bosch, D., Bruguier, O., 2007. Record of a Palaeogene syn-collisional extension in the north Aegean region: evidence from the Kemer micaschists (NW Turkey). Geological Magazine 144, 393–400.

Bonev, N., Burg, J.-P., Ivanov, Z., 2006. Mesozoic–Tertiary structural evolution of an extensional gneiss dome—the Kesebir–Kardamos dome, eastern Rhodope (Bulgaria–Greece). International Journal of Earth Sciences 95, 318–340.

Brun J.-P., Sokoutis, D., 2010. 45 m.y. of Aegean crust and mantle fl ow driven by trench retreat. Geology 38, 815–818.

Burg, J.-P., Ricou, L.-E., Ivanov, Z., Godfriaux, I., Dimov, D., Klain, L. 1996. Syn-metamorphic nappe complex in the Rhodope Massif: structure and kinematics. Terra Nova 8, 6–15.

Chakrabarti, R., Basu, A.R., Ghatak, A., 2012. Chemical geodynamics of Western Anatolia. International Geology Review 54, 227–248.

Christofides, G., Pécskay, Z., Eleftheriadis, G., Soldatos, T., Koroneos, A., 2004. The Tertiary Evros volcanic rocks (Thrace, Northeastern Greece): Petrology and K/Ar Geochronology. Geologica Carpathica 55, 397–409.

Delaloye, M., Bingöl, E., 2000. Granitoids from Western and Northwestern Anatolia: Geochemistry and Modeling of Geodynamic Evolution. International Geology Review 42, 241–268.

DePaolo, D.J., 1981. Trace Element and Isotopic Effects of Combined Wallrock Assimilation and Fractional Crystallization. Earth and Planetary Science Letters 53, 189–202.

Dinter, D.A., 1998. Late Cenozoic extension of the Alpine collisional orogen, northeastern Greece: Origin of the north Aegean basin. Geological Society of America Bulletin 110, 1208–1230.

Dönmez, M., Akçay, A.E., Genç, Ş.C., Acar, Ş., 2005. Biga Yarımadasında Orta-Üst Eosen Volkanizması ve Denizel İgnimbiritler. Bulletin of the Mineral Research and Exploration (Turkey) 131, 49–61.

Ellam, R.M., 1992. Lithospheric thickness as a control on basalt geochemistry. Geology 20, 153–156.

Elmas, A., 2011. The Thrace Basin: stratigraphic and tectonic palaeogeographic evolution of the Palaeogene formations of northwest Turkey. International Geology Review 54, 1419–1442.

Ercan, T., Satir, M., Steinitz, G., Dora, A., Sarifakıoğlu, E., Adis, C., Walter, H.-J., Yıldırım, T., 1995. Biga yarımadasi ile Gökçeada, Bozcaada ve Tavşan adalarındaki (KB Anadolu) Tersiyer volkanizmasinin ozellikleri. Bulletin of the Mineral Research and Exploration (Turkey) 117, 55–86. (*In Turkish*)

Ercan, T., Türkecan, A., Guillou, H., Satır, M., Sevin, D., Şaroğlu, F., 1998. Marmara Denizi çevresindeki Tersiyer volkanizmasının özellikleri. Bulletin of the Mineral Research and Exploration (Turkey) 120, 199–221. (*In Turkish*)

Ersoy, E.Y., Çemen, İ., Helvacı, C., Billor, Z., 2014. Tectono-stratigraphy of the Neogene basins in Western Turkey: Implications for tectonic evolution of the Aegean Extended Region. Tectonophysics 635, 33–58.

Ersoy, E.Y., Palmer, M.R. 2013. Eocene-Quaternary magmatic activity in the Aegean: Implications for mantle metasomatism and magma genesis in an evolving orogeny. Lithos 180-181, 5–24.

Genç, Ş.C., 1998. Evolution of the Bayramic¸ Magmatic Complex, Northwestern Anatolia. Journal of Volcanology and Geothermal Research 85, 233–249.

Genç, Ş.C., 2001. Garnet occurrence in andesitic lavas of Kızderbent volcanics, Armutlu peninsula, NW Turkey. in: Dora, O.Ö., Özgenç, İ., Sözbilir, H. (Eds.), Proceedings of the International Earth Sciences Colloquium on the Aegean Region (IESCA-2000), Dokuz Eylül University, İzmir, Turkey, 25–29 September 2000, 57–62.

Genç, Ş.C., Dönmez, M., Akçay, A.E., Altunkaynak, Ş., Eyüpoğlu, M., Ilgar, Y., 2012. Biga Yarımadası Tersiyer volkanizmasının stratigrafik, petrografik ve kimyasal özellikleri, in Yüzer, E., Tunay, G., (Eds.), Biga Yarımadasının Genel ve Ekonomik Jeolojisi. Bulletin of the Mineral Research and Exploration Special Publications 28, 122–162.

Genç, Ş.C., Yılmaz, Y., 1997. An example of postcollisional magmatism in Northwestern Anatolia: the Kızderbent volcanic (Armutlu peninsula, Turkey). Turkish Journal of Earth Science 6, 33–42.

Georgiev, S., von Quadt, A., Heinrich, C.A., Peytcheva, I., Marchev, P., 2012. Time evolution of a rifted continental arc: Integrated ID-TIMS and LA-ICPMS study of magmatic zircons from the Eastern Srednogorie, Bulgaria. Lithos 154, 53–67.

Gülmez, F., Genç, Ş.C., Keskin, M., Tüysüz, O., 2012. A post-collision slab-breakoff model for the origin of the Middle Eocene magmatic rocks of the Armutlu–Almacık belt, NW

Turkey and its regional implications. Geological Society of London, Special Publications 372, 107–139.

Gülmez, F., Genç, Ş.C., Prelevic, D., Tüysüz, O., Karacık, Z., Roden, M.F., Billor, Z., 2016. Ultrapotassic Volcanism from the Waning Stage of the Neotethyan Subduction: a Key Study from the Izmir–Ankara–Erzincan Suture Belt, Central Northern Turkey. Journal of Petrology 57, 561–593.

Irvine, T.N., Baragar, W.R.A., 1971, A guide to the chemical classification of the common volcanic rocks: Canadian Journal of Earth Sciences 8, 523–548.

Ishizuka, O., Taylor, R.N., Yuasa, M., Milton, J.A., Nesbitt, R.W., Uto, K., Sakamoto, I., 2007. Processes controlling along-arc isotopic variation of the southern Izu-Bonin arc. Geochemistry, Geophysics, Geosystems 8, Q06008.

Johnson, M.C., Plank, T., 1999. Dehydration and melting experiments constrain the fate of subducted sediments, Geochemistry, Geophysics, Geosystems 1(1) 1999GC000014.

Jolivet, L., Brun, J.-P., 2010. Cenozoic geodynamic evolution of the Aegean. International Journal of Earth Science 99, 109–138.

Karacık, Z., Yılmaz, Y., Pearce, J.A., Ece, Ö.I., 2008. Petrochemistry of the south Marmara granitoids, northwest Anatolia, Turkey. International Journal of Earth Sciences 97, 1181–1200.

Kasapoğlu, B., Ersoy, E.Y., Uysal, İ., Palmer, M.R., Zack, T., Koralay, O.E., Karlsson, A., 2016. The Petrology of Paleogene Volcanism in the Central Sakarya, Nallıhan Region (NW Anatolia): Implications for the Initiation and Evolution of Post-Collisional, Slab Break-off Related Magmatic Activity. Lithos 246-247, 81–98.

Keto, L.S., Jacobsen, S.B., 1988. Nd isotopic variations of Phanerozoic paleo-oceans. Earth and Planetary Science Letters 90, 395–410.

Kilias, A., Falalakis, G., Mountrakis, D., 1999. Cretaceous–Tertiary structures and kinematics of the Serbomacedonian metamorphic rocks and their relation to the exhumation of the Hellenic hinterland (Macedonia, Greece). International Journal of Earth Sciences 88, 513–531.

Kilias, A., Falalakis, G., Sfeikos, A., Papadimitriou, E., Vamvaka, A., Gkarlaouni, C., 2013. The Thrace basin in the Rhodope province of NE Greece — A tertiary supradetachment basin and its geodynamic implications. Tectonophysics 595–596, 90–105.

Kinzler, R.J., 1997. Melting of mantle peridotite at pressures approaching the spinel to garnet transition: application to mid-ocean ridge basalt petrogenesis. Journal of Geophysical Research 102, 853–874.

Klein, E.M., 2004. Geochemistry of the Igneous Oceanic Crust. In: Treatise on Geochemistry. Holland, H.D. and Turekian, K.K. (Eds.), Elsevier Amsterdam 3, pp 433-463.

Kürkçüoğlu, B., Furman, T., Hanan, B., 2008. Geochemistry of postcollisional mafic lavas from the North Anatolian Fault zone, Northwestern Turkey. Lithos 101, 416–434.

LeMaitre, R.W., 2002. Igneous rocks: a classification and glossary of terms: recommendations of the International Union of Geological Sciences, Subcommission on the Systematics of Igneous Rocks, Cambridge University Press.

Liew, T.C., McCulloch, M.T., 1985. Genesis of granitoid batholiths of Peninsular Malaysia and implications for models of crustal evolution: Evidence from a Nd-Sr isotopic and U-Pb, zircon study. Geochimica et Cosmochimica Acta 49, 587–600.

Lips, A.L.W., White, S.H., Wijbrans, J.R., 2000. Middle-Late Alpine thermotectonic evolution of the southern Rhodope Massif, Greece, Geodinamica Acta 13, 281–292.

Marchev, P., Raicheva, R., Downes, H., Vaselli, O., Chiaradia, M., Moritz, R., 2004. Compositional diversity of Eocene–Oligocene basaltic magmatism in the Eastern Rhodopes, SE Bulgaria: implications for genesis and tectonic setting. Tectonophysics 393, 301– 328.

Marchev, P., Georgiev, S., Zajacz, Z., Manetti, P., Raicheva, R., von Quadt, A., Tommasini, S., 2009. High-K ankaramitic melt inclusions and lavas in the Upper Cretaceous Eastern Srednogorie continental arc, Bulgaria: Implications for the genesis of arc shoshonites. Lithos 113, 228–245.

Münker, C., 2000. The Isotope and Trace Element Budget of the Cambrian Devil River Arc System, New Zealand: Identification of Four Source Components. Journal of Petrology 41, 759–788.

Nesbitt, H.W., Young, G.M. 1982, Early Proterozoic climates and plate motions inferred from major element chemistry of lutites. Nature 299, 715–717.

Norman, M.D., Garcia, M.O., 1999. Primitive magmas and source characteristics of the Hawaiian plume: petrology and geochemistry of shield picrites. Earth and Planetary Science Letters 168, 27–44.

Ohta, T., Arai, H., 2007. Statistical empirical index of chemical weathering in igneous rocks: a new tool for evaluating the degree of weathering. Chemical Geology 240, 280–297.

Okay, A.I., Satır, M., Maluski, H., Siyako, M., Monie, P., Metzger, R., Akyüz, S., 1996. Paleo- and Neo- Tethyan events in northwest Turkey: Geological and geochronological constraints. In: Yin, A., Harrison, M. (Eds.), Tectonics of Asia. Cambridge University Press: 420–441.

Okay, A.I., Tansel, İ., Tüysüz, O., 2001. Obduction, subduction and collision as reflected in the Upper Cretaceous–Lower Eocene sedimentary record of western Turkey. Geological Magazine 138, 117–142.

Okay, A.I., Satır, M., 2000a. Upper Cretaceous Eclogite-Facies Metamorphic Rocks from the Biga Peninsula, Northwest Turkey. Turkish Journal of Earth Sciences 9, 47–56.

Okay, A.I., Satır, M., 2000b. Coeval plutonism and metamorphism in a latest Oligocene metamorphic core complex in northwest Turkey. Geological Magazine 138, 495–516.

Özcan, Z., Okay, A.I., Özcan, E., Hakyemez, A., Özkan-Altıner, S., 2012. Late Cretaceous–Eocene Geological Evolution of the Pontides Based on New Stratigraphic and Palaeontologic Data between the Black Sea Coast and Bursa (NW Turkey). Turkish Journal of Earth Sciences 21, 933–960.

Palme, H., O'Neill, H.St.C., 2004. Cosmochemical estimates of mantle composition, in: Holland, H.D., Turekian, K.K. (Eds.), Treatise on Geochemistry, Elsevier, Amsterdam, 2 pp 1–38.

Pearce, J.A., 1996. A users guide to basalt discrimination diagrams. In: Wyman, D. A. (Eds.), Trace Element Geochemistry of Volcanic Rocks: Applications for Massive Sulphide Exploration. Geological Association of Canada, Short Course Notes 12, 79–113.

Pearce, J.A., 2008. Geochemical fingerprinting of oceanic basalts with applications to ophiolite classification and the search for Archean oceanic crust. Lithos 100, 14–48.

Peccerillo, R., Taylor, S.R., 1976. Geochemistry of Eocene calc-alkaline volcanic rocks from the Kastamonu area, northern Turkey. Contributions to Mineralogy and Petrology 58, 63–81.

Pourteau, A., Oberhänsli, R., Candan, O., Barrier, E., Vrielynck, B., 2016. Neotethyan closure history of western Anatolia: a geodynamic discussion. International Journal of Earth Sciences 105, 203–224.

Ricou, L.E., Burg J.-P., Godfriaux, I., Ivanov, Z. 1998. Rhodope and vardar: the metamorphic and the olistostromic paired belts related to the Cretaceous subduction under Europe. Geodinamica Acta 11, 285–309.

Robertson, A.H.F., Ustaömer, T., 2004. Tectonic evolution of the Intra-Pontide suture zone in the Armutlu Peninsula, NW Turkey. Tectonophysics 381, 175–209.

Romer, R.L., Forster, H.-J., Breitkreuz, C., 2001. Intracontinental extensional magmatism with a subduction fingerprint: the late Carboniferous Halle Volcanic Complex (Germany). Contributions to Mineralogy and Petrology 141, 201–221.

Saner, S., 1980. Explanation of the development of the Western Pontid mountains and adjacent basins, based on plate tectonic theory, northwestern Turkey. Bulletin of the Mineral Research and Exploration Turkey 93–94, 1–21.

Siyako, M., Huvaz, O., 2007. Eocene stratigraphic evolution of the Thrace Basin, Turkey. Sedimentary Geology 198, 75–91.

Şengör, A.M.C., Yılmaz, Y., 1981. Tethyan evolution of Turkey: a plate tectonic approach. Tectonophysics 75, 181–241.

Turgut S., Türkaslan M., Perinçek D., 1991. Evolution of the Thrace sedimentary basin and its hydrocarbon prospectivity. In A. M. Spencer, Generation, Accumulation and Production of Europe's Hydrogarbons (pp. 415-437), Special Publication of the European Association of Petroleum Geoscientists Vol. 1.

Ustaömer, P.A., Ustaömer, T., Collins, A.S., Reischpeitsch, J., 2009. Lutetian arc-type magmatism along the southern Eurasian margin: New U-Pb LA-ICPMS and whole-rock geochemical data from Marmara Island, NW Turkey. Mineralogy and Petrology 96, 177–196.

van Hinsbergen, D.J.J., Hafkenscheid, E., Spakman, W., Meulenkamp, J.E., Wortel, R., 2005. Nappe stacking resulting from subduction of oceanic and continental lithosphere below Greece. Geology 33, 325–328.

von Quadt, A., Moritz, R., Peytcheva, I., Heinrich, C., 2005. Geochronology and geodynamics of Late Cretaceous magmatism and Cu–Au mineralization in the Panagyurishte region of the Apuseni–Banat–Timok–Srednogorie belt (Bulgaria). Ore Geology Reviews 27, 95–126.

Workman, R.K., Hart, S.R., 2005. Major and trace element composition of the depleted MORB mantle (DMM). Earth and Planetary Science Letters 231, 53–72.

Workman, R.K., Hart, S.R., Jackson, M., Regelous, M., Farley, K.A., Blusztajn, J., Kurz, M. Staudigel, H., 2004. Recycled metasomatized lithosphere as the origin of the Enriched Mantle II (EM2) end-member: Evidence from the Samoan Volcanic Chain. Geochemistry, Geophysics, Geosystems 5, Q04008.

Yılmaz, Y., Genç, Ş.C., Karacık, Z., Altunkaynak, Ş., 2001, Two contrasting magmatic associations of NW Anatolia and their tectonic significance, Journal of Geodynamics 31/3, 243–271.

Yılmaz-Şahin, S., Aysal, N., Güngör, Y., 2012. Petrogenesis of Late Cretaceous Adakitic Magmatism in the İstanbul Zone (Çavuşbaşı Granodiorite, NW Turkey). Turkish Journal of Earth Sciences 21, 1029–1045.

Zou, H.B., 1998. Trace element fractionation during modal and non-modal dynamic melting and open-system melting: a mathematical treatment. Geochimica et Cosmochimica Acta 62, 1937–1945.

Figure Captions

Figure 1. Simplified geological map of Northern Aegean to NW Anatolia, showing the main structures, basement rocks and magmatic suites with available ages (Compiled from the studies referenced in the Geological Setting section in the text.). VS: Vardar suture, IPS: Intra-Pontide suture and IAS: Izmir-Ankara suture. IBTZ: İzmir-Balıkesir Transfer Zone.

Figure 2. Geological map of the Biga Peninsula and its environs in NW Anatolia (compiled from the studies referenced in the Geological Setting section in the text).

Figure 3. Simplified geological map of the Central Sakarya region (compiled from the studies referenced in the Geological Setting section in the text).

Figure 4. Representative photomicrographs of studied rocks: (a) and (b) basalt and andesite samples from the Balıklıçeşme volcanics and (c) a rhyolite from the Kirazlı volcanics. (d) a basalt sample from the Kızderbent volcanics. amp: amphibole; bt: biotite, cpx: clinopyroxene; ol: olivine; pl: plagioclase; sa: sanidine.

Figure 5. Alteration indexes (Chemical Index of Alteration, CIA) and related plots for the samples analysed in this study. (a) Al_2O_3 – $CaO+Na_2O$ – K_2O ternary plot of Nesbitt and Young (1982); (b) FMW ternary plot of Ohta and Arai (2007). [**M** = – 0.395 × ln(SiO_2) + 0.206 × ln(TiO_2) – 0.316 × ln(Al_2O_3) + 0.160 × ln(Fe_2O_3) + 0.246 × ln(MgO) + 0.368 × ln(CaO) + 0.073 × ln(Na_2O) – 0.342 × ln(K_2O) + 2.266; **F** = 0.191 × ln(SiO_2) – 0.397 × ln(TiO_2) + 0.020 × ln(Al_2O_3) – 0.375 × ln(Fe_2O_3) – 0.243 × ln(MgO) + 0.079 × ln(CaO) + 0.392 × ln(Na_2O) + 0.333 × ln(K_2O) – 0.892; **W** = 0.203 × ln(SiO_2) + 0.191 × ln(TiO_2) + 0.296 × ln(Al_2O_3) + 0.215 × ln(Fe_2O_3) – 0.002 × ln(MgO) – 0.448 × ln(CaO) – 0.464 × ln(Na_2O) + 0.008 × ln(K_2O) – 1.374].

Figure 6. Whole rock classification and discrimination plots of the studied rock groups. (a) Total alkali–silica (TAS) classification diagram with IUGS fields after LeMaitre et al. (2002). Alkaline-sub-alkaline discrimination is after Irvine and Baragar, (1971). (b) Zr/Ti versus Nb/Y plot of Pearce (1996); (c) K_2O versus SiO_2 plot of Pecceriollo and Taylor (1976); (d) K_2O versus Na_2O diagram (Le Maitre et al., 2002); (e) Ol' – Ne' – Q' ternary plot of the samples, where **Ol'** = Ol + [0.714 –(Fe/(Fe+Mg))0.067]En; **Ne'** = Ne + 0.542Ab; **Q'** = Q + 0.4Ab + 0.25En, based on normative mineralogy. Literature data are from Kasapoğlu et al.

(2016); Gülmez et al. (2013); Kürkçüoğlu et al. (2008); Chakrabarti et al. (2012); Genç and Yılmaz (1997); Altunkaynak and Genç (2008); Ercan et al. (1995, 1998); Aldanmaz et al. (2000); Akal (2013). A: andesite, aB: alkali basalt, aR: alkali rhyolite, B: basalt, BA: basaltic andesite, Bta: basaltic trachyandesite, D: dacite, F: foidite, Ph: phonolite, Pht: phonotephrite, R: rhyolite, T/Td: trachyte/trachydacite, Tb: trachybasalt, Tph: tephriphonolite, Te/Bs: tephrite/basanites,

Figure 7. Whole rock SiO_2-dependent major element variation plots of the studied rock groups. See Figure 6 for symbols. BOVR: Biga orogenic volcanic rocks; KV: Kızderbent volcanics of the SOVR (Sakarya orogenic volcanic rocks), including local Miocene basaltic extrusives.

Figure 8. Whole rock SiO_2-dependent trace element variation plots of the studied rock groups. See Figure 6 for symbols. BOVR: Biga orogenic volcanic rocks; KV: Kızderbent volcanics of the SOVR (Sakarya orogenic volcanic rocks), including local Miocene basaltic extrusives.

Figure 9. (a-d) age-dependent geochemical variation plots of the studied rock groups. See Figure 6 for symbols. BOVR: Biga orogenic volcanic rocks; SOVR: Sakarya orogenic volcanic rocks (including both the Eocene Nallıhan volcanics and Miocene basaltic extrusives).

Figure 10. Whole-rock N-MORB (Normal Mid-Ocean Ridge Basalts)- normalized multi-element diagram of the studied rock groups. N-MORB normalizing values are from Klein (2004).

Figure 11. Whole-rock Sr, Nd and Pb isotopic variations of the studied rock groups. (a) $^{143}Nd/^{144}Nd_{(I)}$ versus $^{87}Sr/^{86}Sr_{(I)}$, (b) $^{87}Sr/^{86}Sr_{(I)}$ versus SiO_2 (wt%), (c) $^{208}Pb/^{204}Pb_{(I)}$ versus

$^{206}Pb/^{204}Pb_{(I)}$, (d) $^{143}Nd/^{144}Nd_{(I)}$ versus $^{206}Pb/^{204}Pb_{(I)}$ plots. Also shown are compositional fields for the NW Anatolia Miocene volcanic rock units. Symbols as in Fig 6.

Figure 12. Whole-rock (a) La/Yb versus La (ppm), (b) Nb/Zr versus Nb (ppm), (c) Nb/La versus SiO_2 (wt%) and (d) Nb/Ba versus SiO_2 (wt%) plots of the studied rock groups. See Symbols as in Fig 6. Also shown are the possible mantle compositions of Primitive Mantle (PM; Palme and O'Neil, 2004), Depleted MORB mantle (DMM), depleted-DMM (D-DMM), Enriched-DMM (E-DMM; Workmann and Hart, 2005). Non-modal closed system dynamic melting trend for the Depleted MORB mantle (DMM), and fractional crystallization trend (FC) of the obtained 2% partial melt is also shown on (b). Melting model uses 1% critical porosity for melt segregation and spinel-facies mantle mineralogy of $ol_{0.53(-0.06)}$ + $opx_{0.27(0.28)}$ + $cpx_{0.17(0.67)}$ + $sp_{0.03(0.11)}$ (Kinzler, 1997), where the numbers indicate mineral (and melt) modes. The partition coefficients are from Adam and Green (2006).

Figure 13. Whole-rock (a) Th/Yb versus Nb/Yb (Pearce, 2008), (b) Ba/Zr versus Nb/Zr, (c) $T_{DMM(2)}$ versus Nb/La and (d) $^{143}Nd/^{144}Nd_{(I)}$ versus Nb/La plots of the studied rock groups. Depleted MORB mantle (DMM), depleted-DMM (D-DMM), Enriched-DMM (E-DMM; Workmann and Hart, 2005), average OIB compositions (Workmann et al., 2004) and OIB source (Norman and Garcia, 1999) are also shown to mark the mantle compositional array on (a), (b) and (d). Non-modal dynamic melting model is also shown on (b) by using D-DMM source composition with spinel-facies mantle mineralogy (Kinzler, 1997) and 1% critical porosity for melt segregation. Second-stage Nd DMM model ages on (c) are calculated according to Keto and Jacobsen (1987). Subduction Fluid (SF) and Subduction Melt (SM) compositions on (d) are calculated by using fluid and melt partition coefficients of Johnson and Plank (1999) and the procedures given in Münker (2000). See Table 3 for calculated compositions of SF1, SF2, SM1 and SM2. Simple mixing curves between SF2 and distinct mantle sources are also shown on (d). FC and AFC vectors are calculated for 90%

crystallization of a mineral assemblage of $olivine_{0.30}$+$clinopyroxene_{0.30}$+$plagioclase_{0.40}$ from a melt represented by the sample C-15. AFC vectors are calculated for r=0.2 and r=0.5 (relative ratio of assimilated material to crystallized material) Composition of assimilating material for the AFC model on (d) is: Nb=12 ppm; La= 40 ppm; $^{143}Nd/^{144}Nd$=0.5120. See text for details and to Figure 6 for symbols.

Figure 14. Tb/Yb vs La/Yb systematics of the studied rock groups. Approximate curves for partial melts from garnet- and spinel-bearing mantle are also shown. See text for details and to Figure 6 for symbols.

Tables

Table 1. Sr and Nd isotopic compositions and related parameters of the studied rock units and the high-pressure metasediments of the Tavşanlı Zone. Kiv: Kızderbent volcanics, BV: Balıklıçeşme volcanics, Krv: Kirazlı volcanics, Hv: Hallaçlar volcanics, TZ: Tavşanlı Zone high-pressure metasediments.

Table 2. Pb isotopic compositions of the studied rock units. Kiv: Kızderbent volcanics, BV: Balıklıçeşme volcanics, Krv: Kirazlı volcanics, Hv: Hallaçlar volcanics.

Table 3. Average geochemistry of the Tavşanlı Zone metasediments (see Appendix 1) and calculated compositions of subduction melts and fluids. Distribution coefficients are from Johnson and Plank (1999).

Supplementary Materials

1 – Age data for the Biga Peninsula and Central Sakarya volcanics

2 – WR major and trace element data

Table 1. Sr and Nd isotopic compositions and related parameters of the studied rock units and the high-pressure metasediments of the Tavşanlı Zone. Kiv: Kızderbent volcanics, BV: Balıklıçeşme volcanics, Krv: Kirazlı volcanics, Hv: Hallaçlar volcanics, TZ: Tavşanlı zone high-pressure metasediments.

Sample	Unit	AGE (Ma)	$^{87}Sr/^{86}Sr$	$^{143}Nd/^{144}Nd$	$^{147}Sm/^{144}Nd$	$^{87}Rb/^{86}Sr$	$^{87}Sr/^{86}Sr_{(i)}$	$^{143}Nd/^{144}Nd_{(i)}$	$\varepsilon Sr_{(i)}$	$\varepsilon Nd_{(i)}$	$f_{Sm/Nd}$(*)	$T_{Nd}^{(DM1)}$(Ma) (**)	$T_{Nd}^{(DM2)}$(Ma) (**)
G-03	KiV	50	0.706358	0.512572	0.12	0.25	0.706181	0.512533	24.66	-0.79	-0.40	927.03	921.22
G-05	KiV	50	0.705361	0.512833	0.18	0.15	0.705253	0.512775	11.49	3.93	-0.10	1317.26	534.45
G-21	KiV	50	0.705708	0.512675	0.14	0.94	0.705044	0.512629	8.53	1.07	-0.28	1006.96	768.78
G-28	KiV	50	0.704838	0.512774	0.13	0.24	0.704668	0.512730	3.18	3.06	-0.32	712.34	607.30
G-45	KiV	50	0.704503	0.512916	0.20	0.11	0.704423	0.512850	-0.30	5.39	0.03	3048.05	411.42
G-48	KiV	50	0.706071	0.512680	0.11	0.48	0.705727	0.512643	18.22	1.36	-0.43	706.01	746.34
B-05	BV	40	0.705863	0.512617	0.15	0.09	0.705811	0.512578	19.39	-0.16	-0.25	1243.58	860.64
B-11	BV	40	0.705429	0.512702	0.12	0.42	0.705192	0.512671	10.60	1.65	-0.40	718.35	714.49
B-12	BV	40	0.706172	0.512582	0.11	0.23	0.706039	0.512553	22.63	-0.66	-0.43	855.48	902.90
B-17	BV	40	0.706501	0.512507	0.13	0.61	0.706153	0.512474	24.25	-2.20	-0.36	1125.65	1027.31
B-24	BV	40	0.705748	0.512595	0.13	0.09	0.705697	0.512561	17.77	-0.51	-0.33	1028.68	889.44
B-32	BV	40	0.705502	0.512659	0.12	0.14	0.705421	0.512627	13.86	0.79	-0.38	817.96	784.26
B-35	BV	40	0.704981	0.512713	0.15	0.04	0.704957	0.512674	7.27	1.71	-0.25	1017.14	708.35
C-15	BV	40	0.706565	0.512490	0.13	0.09	0.706512	0.512456	29.34	-2.55	-0.34	1212.39	1055.74
C-22	BV	40	0.705979	0.512625	0.13	0.05	0.705952	0.512592	21.40	0.10	-0.35	928.71	840.33
C-40	BV	40	0.704874	0.512728	0.13	0.16	0.704783	0.512694	4.80	2.09	-0.33	778.23	678.00
C-42	BV	40	0.706071	0.512595	0.12	0.35	0.705875	0.512565	20.29	-0.43	-0.41	866.07	883.60
B-21	Krv	30	0.706672	0.512643	0.13	2.97	0.705408	0.512618	13.65	0.37	-0.36	877.97	810.23
B-27	Krv	30	0.706670	0.512509	0.10	0.41	0.706496	0.512489	29.10	-2.16	-0.48	882.59	1016.84
C-07	Krv	30	0.705496	0.512631	0.13	0.45	0.705304	0.512606	12.18	0.13	-0.36	909.22	829.58
C-09	Krv	30	0.707282	0.512447	0.12	0.58	0.707035	0.512424	36.74	-3.42	-0.41	1104.19	1119.01
C-31	Krv	30	0.705906	0.512608	0.11	0.68	0.705616	0.512586	16.60	-0.27	-0.42	827.39	862.54
C-36	Krv	30	0.705835	0.512642	0.11	0.88	0.705459	0.512620	14.38	0.40	-0.43	765.32	808.10
C-39	Krv	30	0.705744	0.512639	0.12	0.52	0.705524	0.512616	15.30	0.33	-0.42	789.77	813.60
HG-1	Hv	25	0.706859	0.512509	0.11	0.43	0.706707	0.512492	32.09	-2.23	-0.46	914.66	1018.51
HG-2	Hv	25	0.707367	0.512470	0.10	0.63	0.707144	0.512453	38.29	-2.97	-0.48	926.12	1079.33
HG-9	Hv	25	0.707100	0.512483	0.10	0.37	0.706969	0.512466	35.80	-2.72	-0.48	910.67	1058.73
M06-140/A	TZ	50	0.723790	0.512124	0.11	2.58	0.721965	0.512088	248.72	-9.48			
M06-143/1	TZ	50	0.724423	0.512096	0.10	1.67	0.723240	0.512062	266.82	-9.98			

(*) $f_{Sm/Nd} = [(^{147}Sm/^{144}Nd)_{sample} / (^{147}Sm/^{144}Nd)_{CHUR}] - 1$, where $(^{147}Sm/^{144}Nd)_{CHUR} = 0.1967$

(**) $T_{Nd}^{(DM1)} = 1 / \lambda \ln\{1 + [(^{143}Nd/^{144}Nd)_{sample} - 0.51315] / [(^{147}Sm/^{144}Nd)_{sample}] - 0.2137$, where λ = decay constants of $^{147}Sm = 0.00654\ Ga^{-1}$.

(***) $T_{Nd}^{(DM2)} = T_{Nd}^{(DM1)} - (T_{Nd}^{(DM1)} - t)\ ((f_{cc} - f_s) / (f_{cc} - f_{DM}))$, where t = age of the sample; f_{cc} = continental crust $f_{Sm/Nd} = -0.4$; f_s = sample $f_{Sm/Nd}$; f_{DM} = depleted mantle $f_{Sm/Nd} = 0.8592$.

Table 2. Pb isotopic compositions of the studied rock units. Kiv: Kızderbent volcanics, BV: Balıklıçeşme volcanics, Krv: Kirazlı volcanics, Hv: Hallaçlar volcanics.

Sample	Unit	AGE (Ma)	Pb	Th	U	$^{206}Pb/^{204}Pb$	$^{207}Pb/^{204}Pb$	$^{208}Pb/^{204}Pb$	$^{206}Pb/^{204}Pb_{(i)}$	$^{207}Pb/^{204}Pb_{(i)}$	$^{208}Pb/^{204}Pb_{(i)}$
G-05	KiV	50	1.14	0.6	0.2	18.738	15.629	38.732	18.650	15.624	38.646
G-28	KiV	50	9.55	6.4	1.6	18.733	15.650	38.804	18.649	15.646	38.694
G-45	KiV	50	4.26	1.5	0.4	18.696	15.637	38.695	18.649	15.634	38.637
G-48	KiV	50	13.33	7.8	2.8	18.804	15.662	38.862	18.699	15.657	38.766
B-05	BV	40	15.42	3.7	1.0	18.933	15.687	38.930	18.907	15.686	38.899
B-11	BV	40	12.06	6.9	1.9	18.924	15.678	38.876	18.861	15.675	38.801
B-12	BV	40	24.32	11.8	3.4	18.864	15.678	38.871	18.808	15.675	38.807
B-17	BV	40	21.27	11.1	3.2	18.857	15.687	38.921	18.796	15.684	38.852
B-35	BV	40	9.73	2.2	0.8	18.868	15.663	38.798	18.835	15.661	38.769
C-15	BV	40	10.46	4.9	1.2	18.823	15.670	38.855	18.777	15.667	38.793
C-42	BV	40	19.52	10.8	3.0	18.887	15.680	38.878	18.826	15.677	38.805
B-21	Krv	30	38.10	27.9	9.9	18.869	15.673	38.911	18.791	15.669	38.839
C-07	Krv	30	22.38	12.2	3.2	18.872	15.673	38.900	18.829	15.671	38.846
C-09	Krv	30	17.21	8.7	2.2	18.877	15.689	38.946	18.839	15.687	38.896
C-31	Krv	30	27.62	21.5	3.8	18.826	15.678	38.884	18.785	15.676	38.807
C-36	Krv	30	23.80	19.4	6.0	18.881	15.674	38.906	18.805	15.670	38.826
HG-2	Hv	25	48.25	34.1	10.0	18.828	15.699	39.011	18.776	15.697	38.953
HG-9	Hv	25	41.48	25.7	5.6	18.800	15.697	38.992	18.766	15.696	38.941

Table 3. Average geochemistry of the Tavşanlı zone metasediments (see Appendix 1) and calculated compositions of subduction melts and fluids. Distribution coefficients are from Jhonson and Plank (1999).

	Sediment composition	melt distribution coefficients		fluid distribution coefficients		Sediment Melts (*)		Sediment Fluids (**)	
	Average TZ	(800 °C)	(900 °C)	(650 °C)	(700 °C)	SM-1 800 °C/0.5%	SM-2 900 °C/1.0%	SF-1 650 °C /0.5%	SF-2 700 °C /0.5%
Cs	3.55	0.56	0.79	1.60	2.34	6.33	4.49	2.22	1.52
Rb	61.55	1.55	0.42	2.00	1.32	39.74	145.54	30.81	46.66
Ba	386.50	1.64	0.48	0.84	1.04	235.90	800.85	459.90	371.67
Sr	85.45	0.67	1.23	0.53	0.91	127.38	69.54	160.87	93.88
Pb	11.75	0.78	n.a.	0.64	0.94	15.05	n.a.	18.33	12.50
Th	8.75	1.45	0.82	4.81	4.13	6.04	10.66	1.82	2.12
U	1.60	1.07	0.62	1.37	3.06	1.50	2.57	1.17	0.52
Ta	0.75	1.51	1.23	2.00	2.72	0.50	0.61	0.38	0.28
Y	15.95	10.70	1.68	1.16	2.93	1.49	9.51	13.75	5.45
Nb	6.45	1.42	1.23	2.65	2.99	4.55	5.25	2.44	2.16
Sc	8.50	9.57	1.81	1.19	4.18	0.89	4.71	7.15	2.04
La	32.75	2.47	1.52	4.00	1.70	13.28	21.58	8.20	19.28
Ce	60.85	2.97	1.30	4.01	1.56	20.52	46.86	15.20	39.04
Pr	6.52	3.73	1.41	3.67	1.48	1.75	4.63	1.78	4.41
Nd	24.50	4.41	1.46	3.26	1.44	5.57	16.81	7.53	17.03
Sm	4.30	4.17	1.62	2.41	1.61	1.03	2.66	1.79	2.67
Eu	0.80	8.11	1.74	2.27	1.56	0.10	0.46	0.35	0.51
Gd	3.72	8.67	1.66	1.76	2.02	0.43	2.24	2.11	1.84
Tb	0.55	9.32	1.72	1.52	2.31	0.06	0.32	0.36	0.24
Dy	3.04	10.00	1.72	1.34	2.60	0.30	1.77	2.27	1.17
Ho	0.56	10.50	1.75	1.20	2.97	0.05	0.32	0.47	0.19
Er	1.64	10.10	1.69	1.14	3.17	0.16	0.97	1.44	0.52
Yb	1.73	9.68	1.68	1.06	3.66	0.18	1.03	1.63	0.47
Lu	0.25	9.28	1.87	1.05	3.85	0.03	0.13	0.23	0.06
$^{87}Sr/^{86}Sr$	0.724107								
$^{143}Nd/^{144}Nd$	0.512110								
$^{87}Sr/^{86}Sr$ (@50 Ma)	0.722602					0.722602	0.7226022	0.722602	0.7226022
$^{143}Nd/^{144}Nd$ (@50 Ma)	0.512075					0.512075	0.5120749	0.512075	0.5120749

(*) Sediment melt compositions are calculated by using accumulated fractional melting equation and the melt distribution coefficients of 800 °C (SM-1 with 0.5% melt fraction) and 900 °C (SM-2 with 1.0% melt fraction). (**) Sediment fluid compositions are calculated by using accumulated fractional melting equation and the fluid distribution coefficients of 650 °C (SF-1 with 0.5% fluid fraction) and 700 °C (SF-2 with 0.5% fluid fraction).

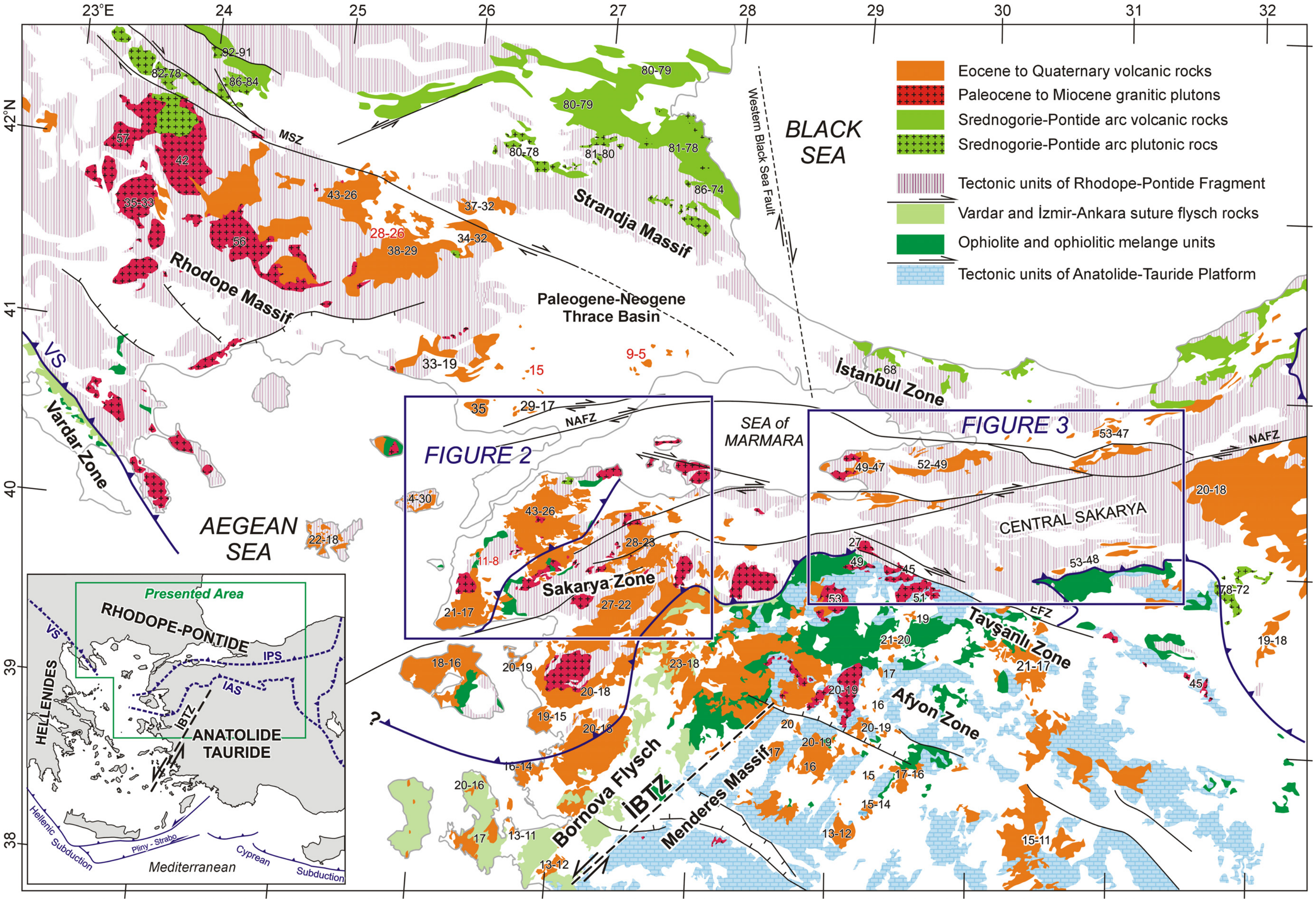

Figure 1. Simplified geological map of Northern Aegean to NW Anatolia, showing the main structures, basement rocks and magmatic suites with available ages (from Ersoy et al. under review). VS: Vardar suture, IPS: Intra-Pontide suture and IAS: Izmir-Ankara suture. IBTZ: İzmir-Balıkesir Transfer Zone.

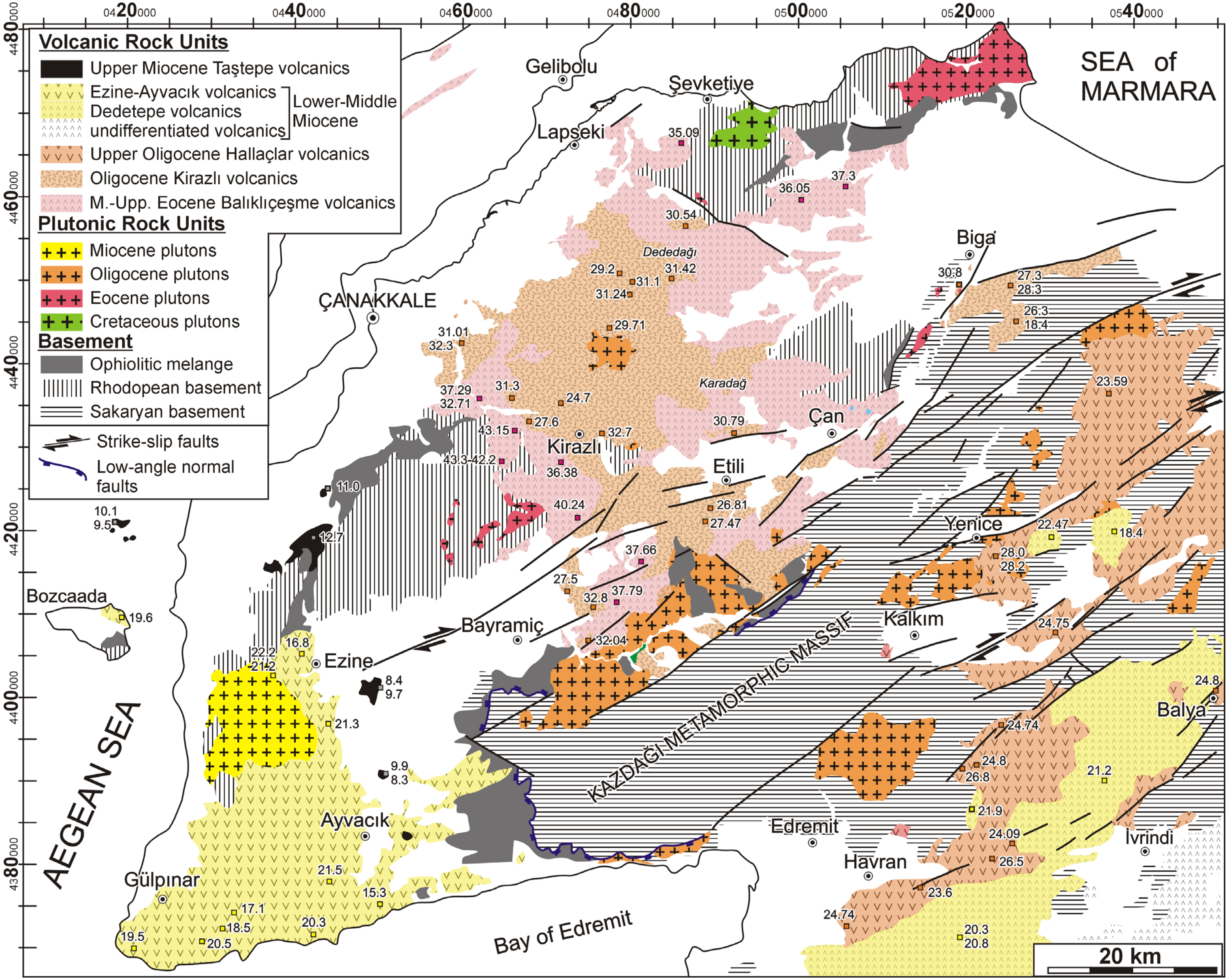

Figure 2. Geological map of the Biga Peninsula and its environs in NW Anatolia (see Ersoy et al. under review for the references for age data).

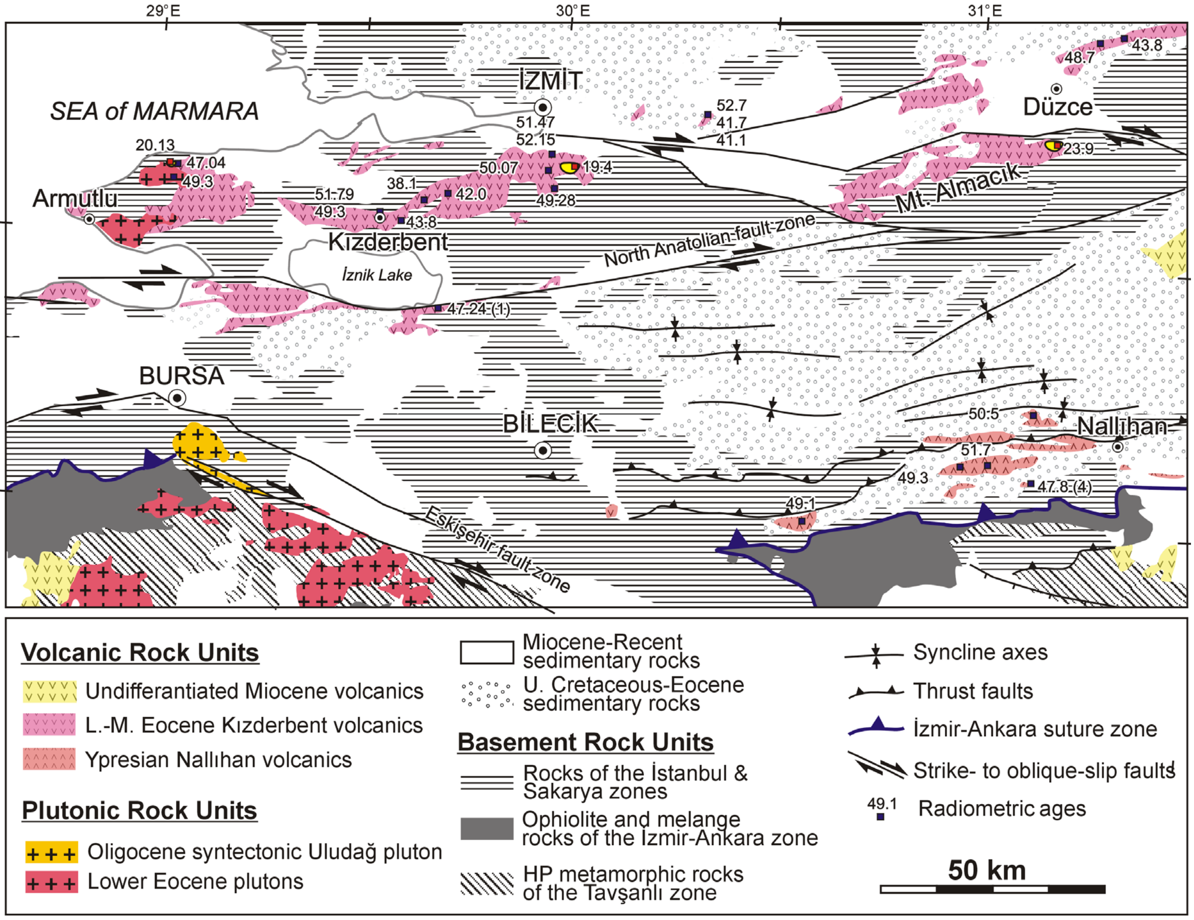

Figure 3. Simplified geological map of the Central Sakarya region. (see Ersoy et al. under review for the references for age data).

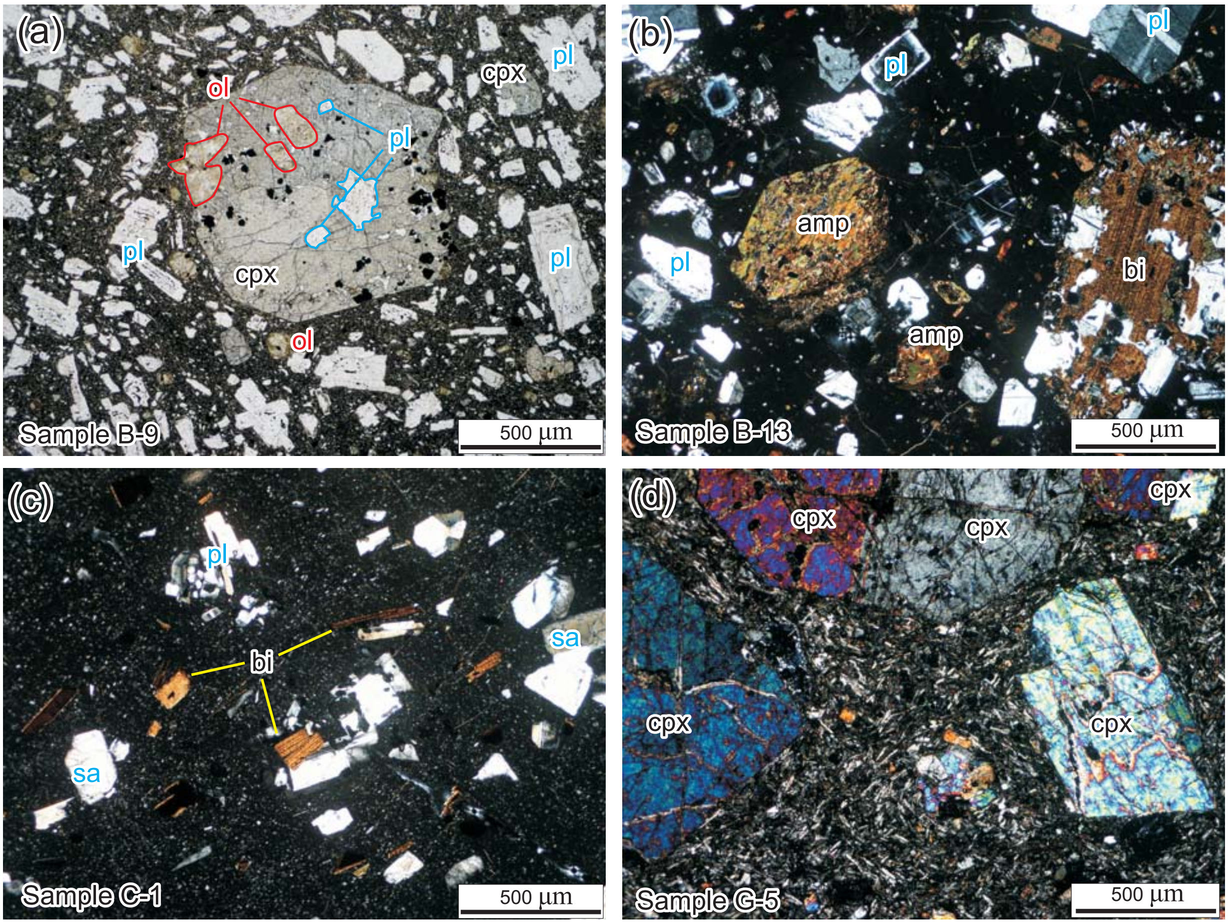

Figure 4. Representative photomicrograps of studied rocks: (a) and (b) basalt and andesite samples from the Balıklıçeşme volcanics and (c) a rhyolite from the Kirazlı volcanics. (d) a basalt sample from the Kızderbent volcanics.

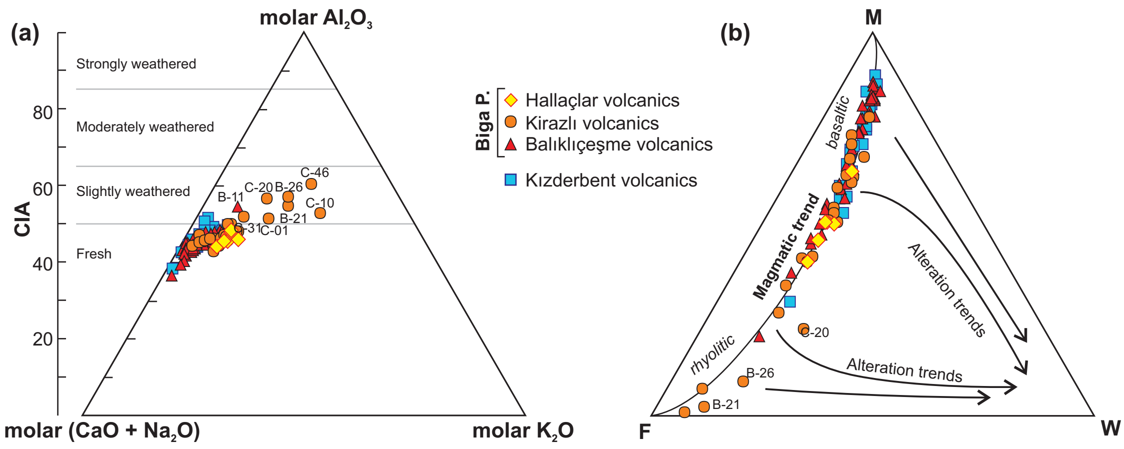

Figure 5. Alteration indexes (Chemical Index of Alteration, CIA) and related plots for the samples analysed in this study. (a) Al2O3 – CaO+Na2O – K2O ternary plot of Nesbitt and Young (1982); (b) FMW ternary plot of Ohta and Arai (2007). [M = –0.395 × ln(SiO2) + 0.206 × ln(TiO2) – 0.316 × ln(Al2O3) + 0.160 × ln(Fe2O3) + 0.246 × ln(MgO) + 0.368 × ln(CaO) + 0.073 × ln(Na2O) – 0.342 × ln(K2O) + 2.266; F = 0.191 × ln(SiO2) – 0.397 × ln(TiO2) + 0.020 × ln(Al2O3) – 0.375 × ln(Fe2O3) – 0.243 × ln(MgO) + 0.079 × ln(CaO) + 0.392 × ln(Na2O) + 0.333 × ln(K2O) – 0.892; W = 0.203 × ln(SiO2) + 0.191 × ln(TiO2) + 0.296 × ln(Al2O3) + 0.215 × ln(Fe2O3) – 0.002 × ln(MgO) – 0.448 × ln(CaO) – 0.464 × ln(Na2O) + 0.008 × ln(K2O) – 1.374].

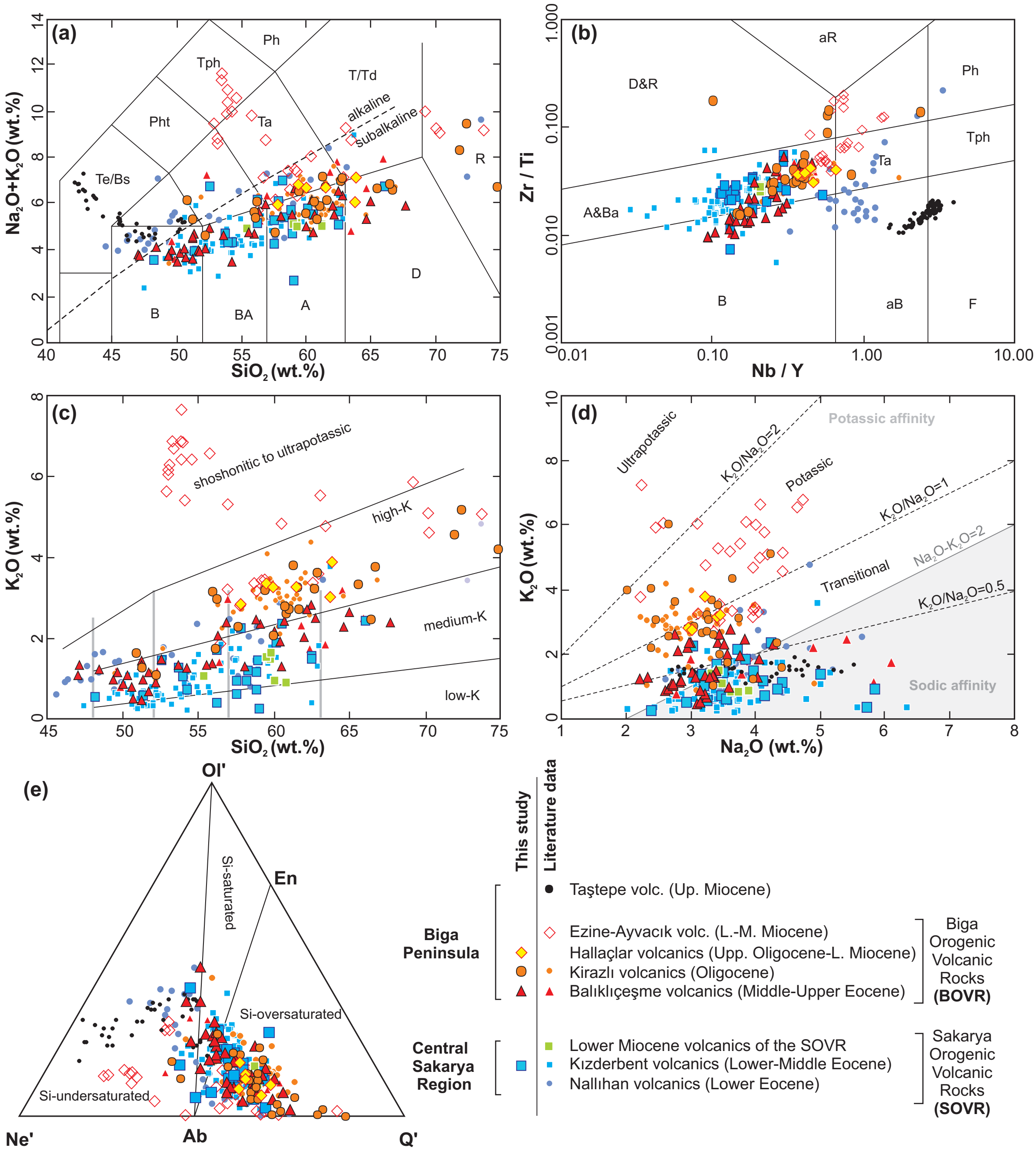

Figure 6. Whole rock classification and discrimination plots of the studied rock groups. (a) Total alkali–silica (TAS) classification diagram with IUGS fields after LeMaitre et al. (2002). Alkaline-sub-alkaline discrimnation is after Irvine and Baragar, (1971). (b) Zr/Ti versus Nb/Y plot of Pearce (1996); (c) K2O versus SiO2 plot of Pecceriollo and Taylor (1976); (d) K2O versus Na2O diagram (Le Maitre et al., 2002); (e) Ol' – Ne' – Q' ternary plot of the samples, where Ol' = Ol + [0.714 –(Fe/(Fe+Mg))0.067]En; Ne' = Ne + 0.542Ab; Q' = Q + 0.4Ab + 0.25En, based on normative mineralogy. Literature data are from Kasapoğlu et al. (2016); Gülmez et al. (2013); Kürkçüoğlu et al. (2008); Chakrabarti et al. (2012); Genç and Yılmaz (1997); Altunkaynak and Genç (2008); Ercan et al. (1995, 1998); Aldanmaz et al. (2000); Akal (2013).

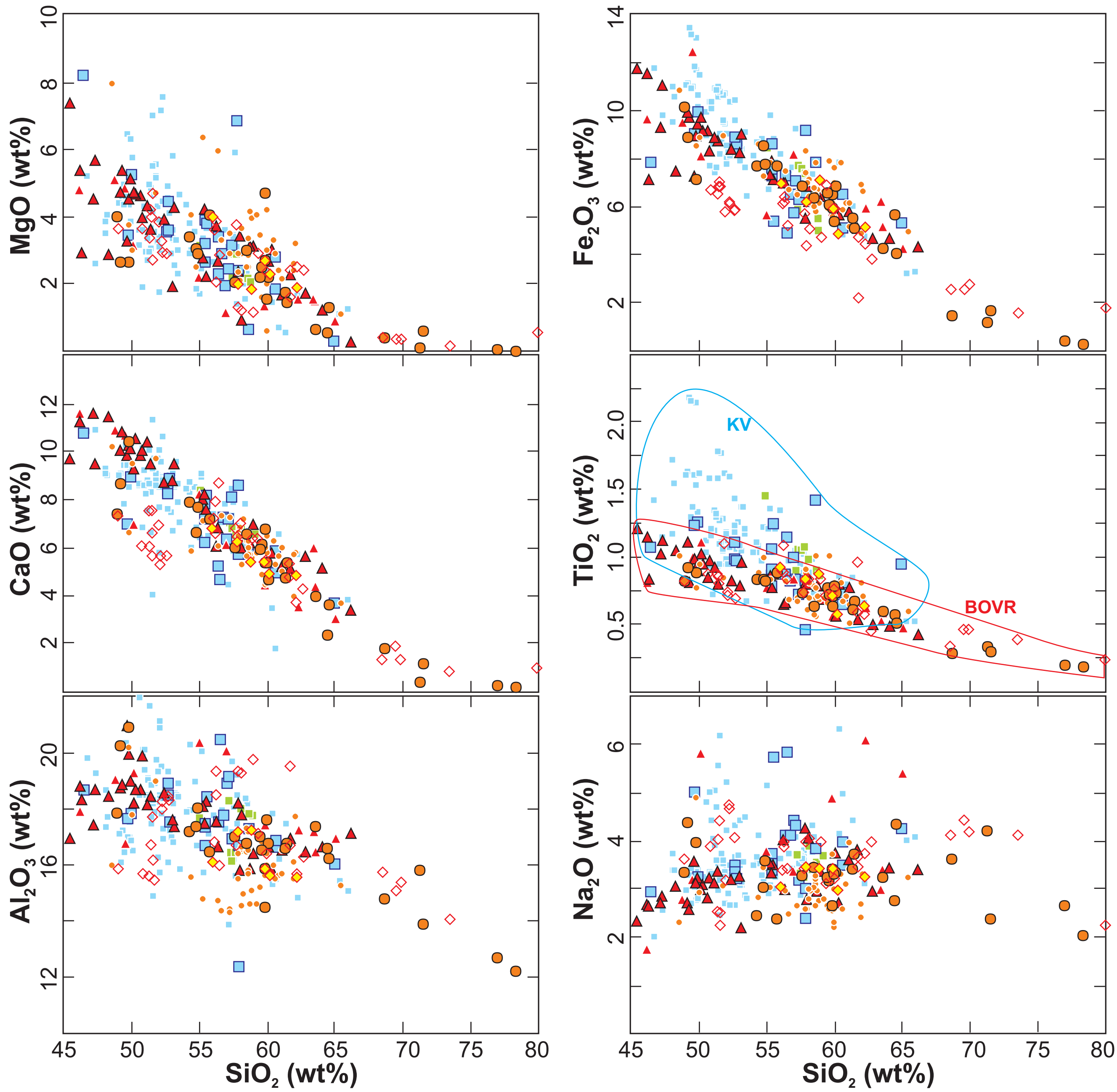

Figure 7. Whole rock SiO2-dependent major element variation plots of the studied rock groups. See Figure 6 for symbols. KV: Kızderbent volcanics together with local Miocene basaltic extrusives.

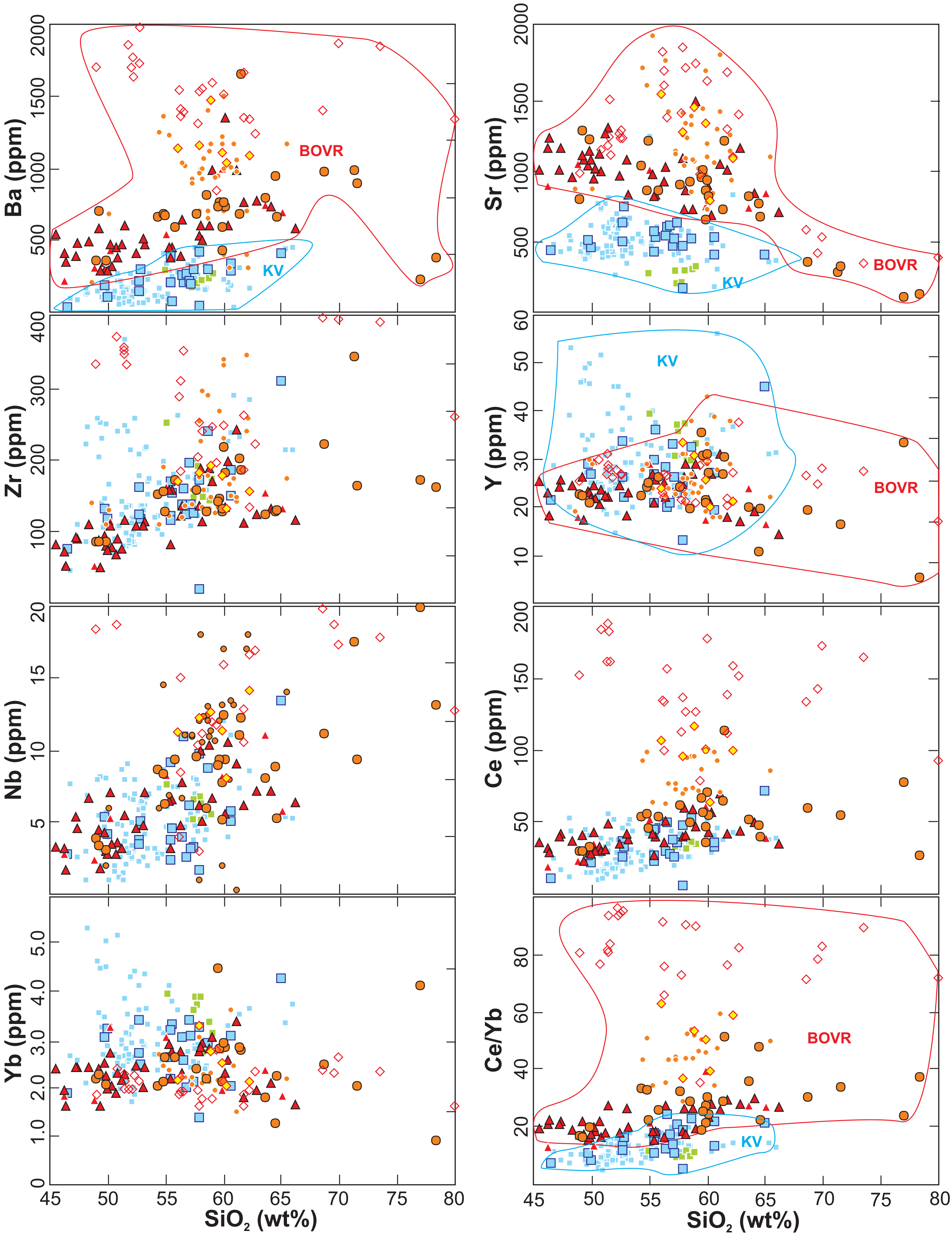

Figure 8. Whole rock SiO2-dependent trace element variation plots of the studied rock groups. See Figure 6 for symbols. KV: Kızderbent volcanics together with local Miocene basaltic extrusives.

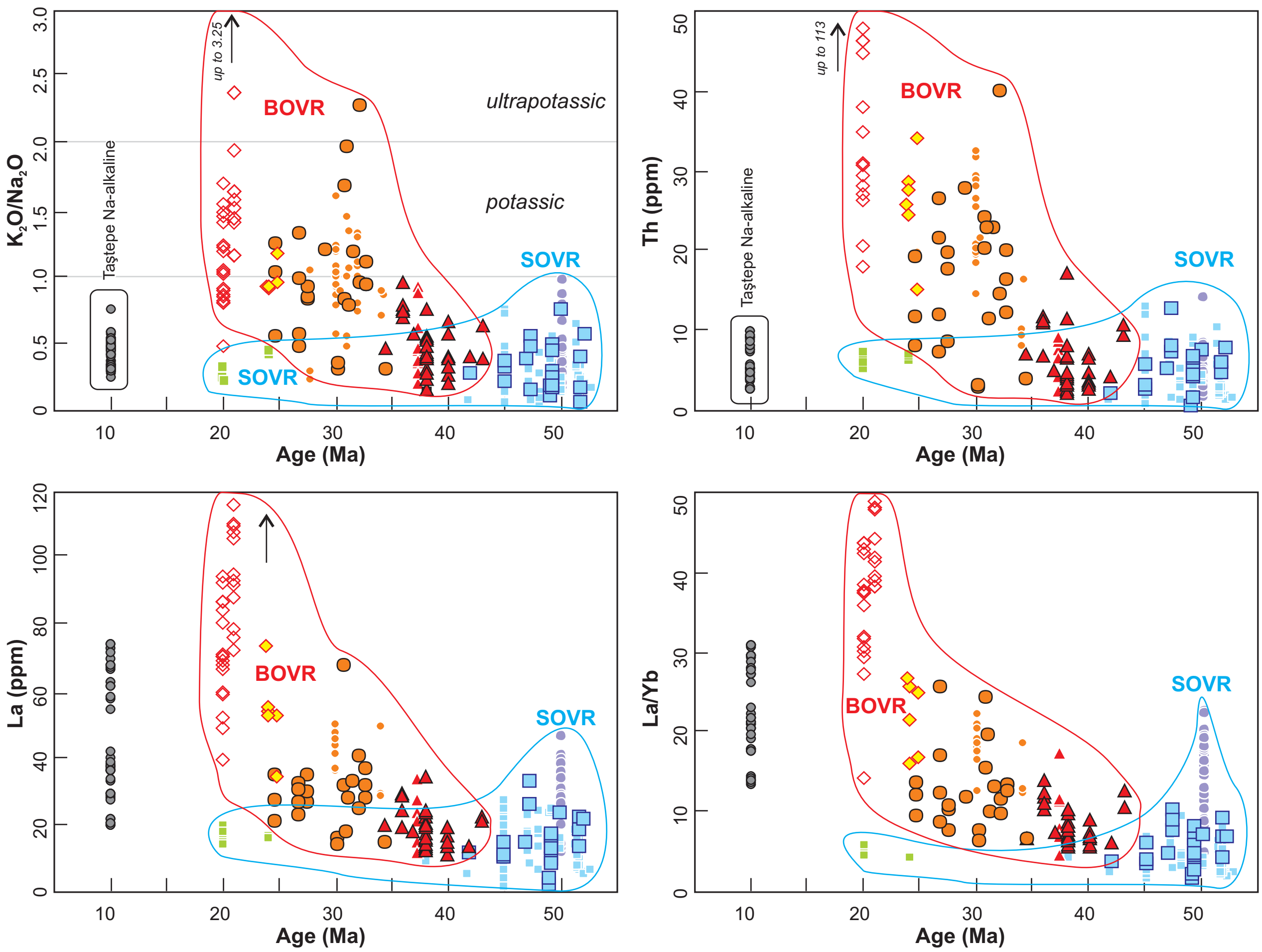

Figure 9. (a-d) age-dependent geochemical variation plots of the studied rock groups. See Figure 6 for symbols. KV: Kızderbent volcanics together with local Miocene basaltic extrusives.

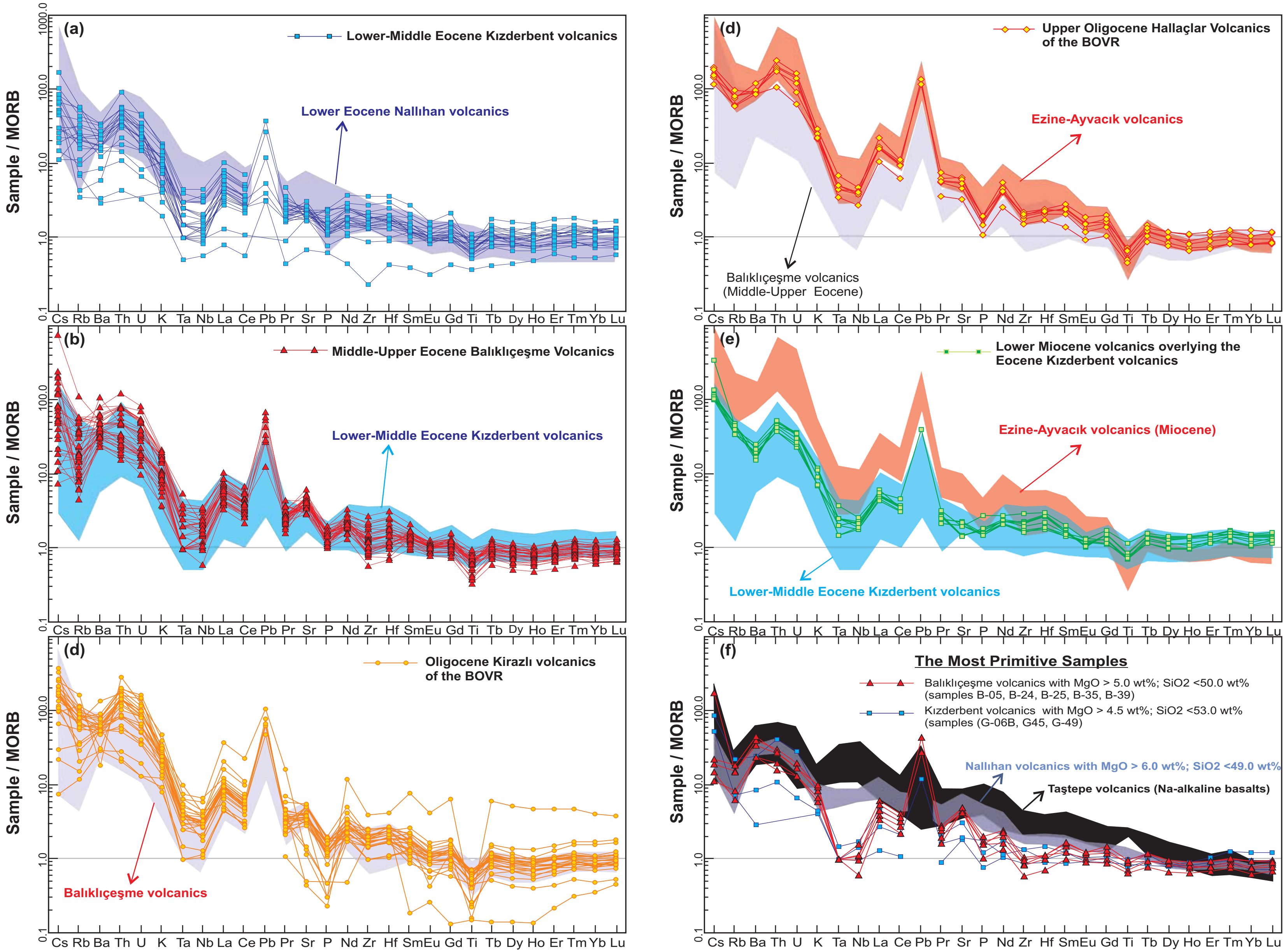

Figure 10. Whole-rock N-MORB (Normal Mid-Ocean Ridge Basalts)- normalized multi-element diagram (b and d) of the studied rock groups. N-MORB normalizing values are from Klein (2004).

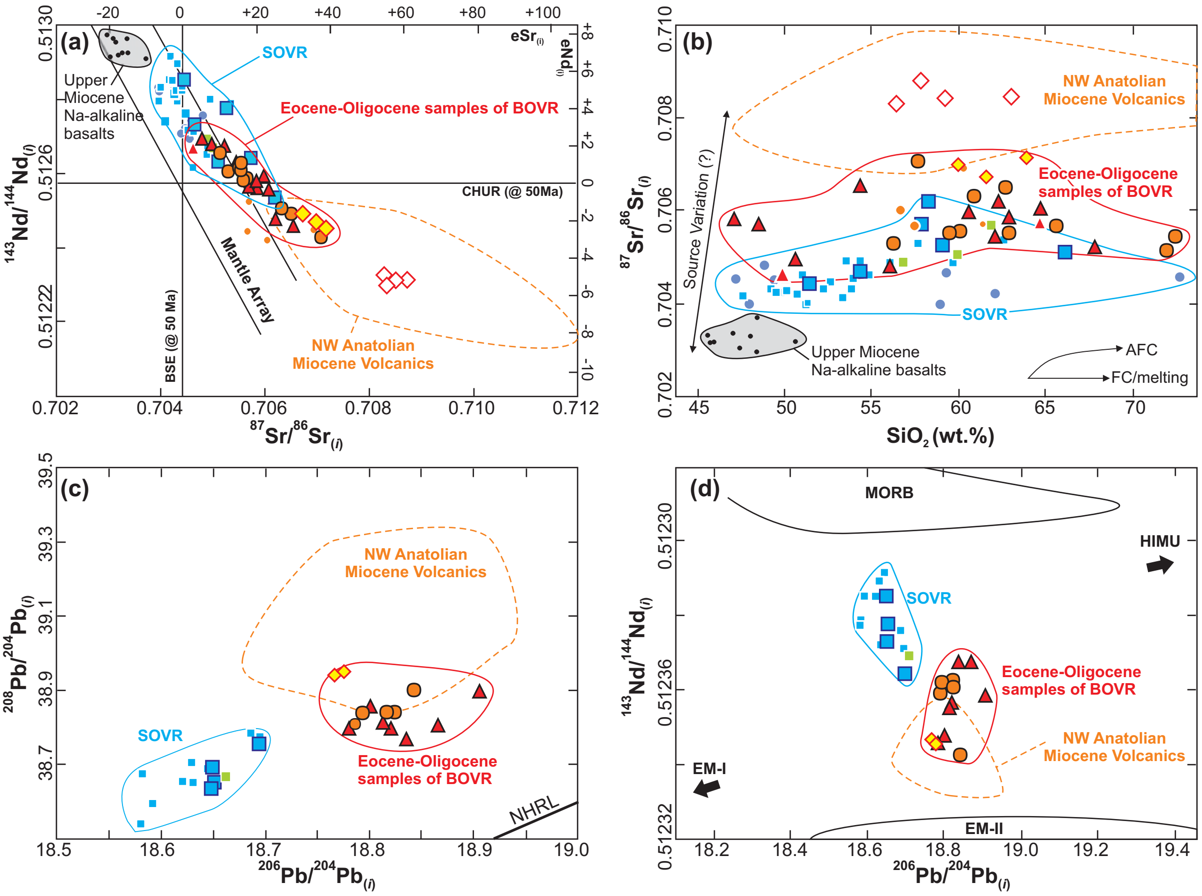

Figure 11. Whole-rock Sr, Nd and Pb isotopic variations of the studied rock groups. (a) 143Nd/144Nd(I) versus 87Sr/86Sr(I), (b) 87Sr/86Sr(I) versus SiO2 (wt%), (c) 208Pb/204Pb(I) versus 206Pb/204Pb(I), (d) 143Nd/144Nd(I) versus 206Pb/204Pb(I) plots. Also shown are compositional fields for the NW Anatolia Miocene volcanic rock units. See Figure 6 for symbols.

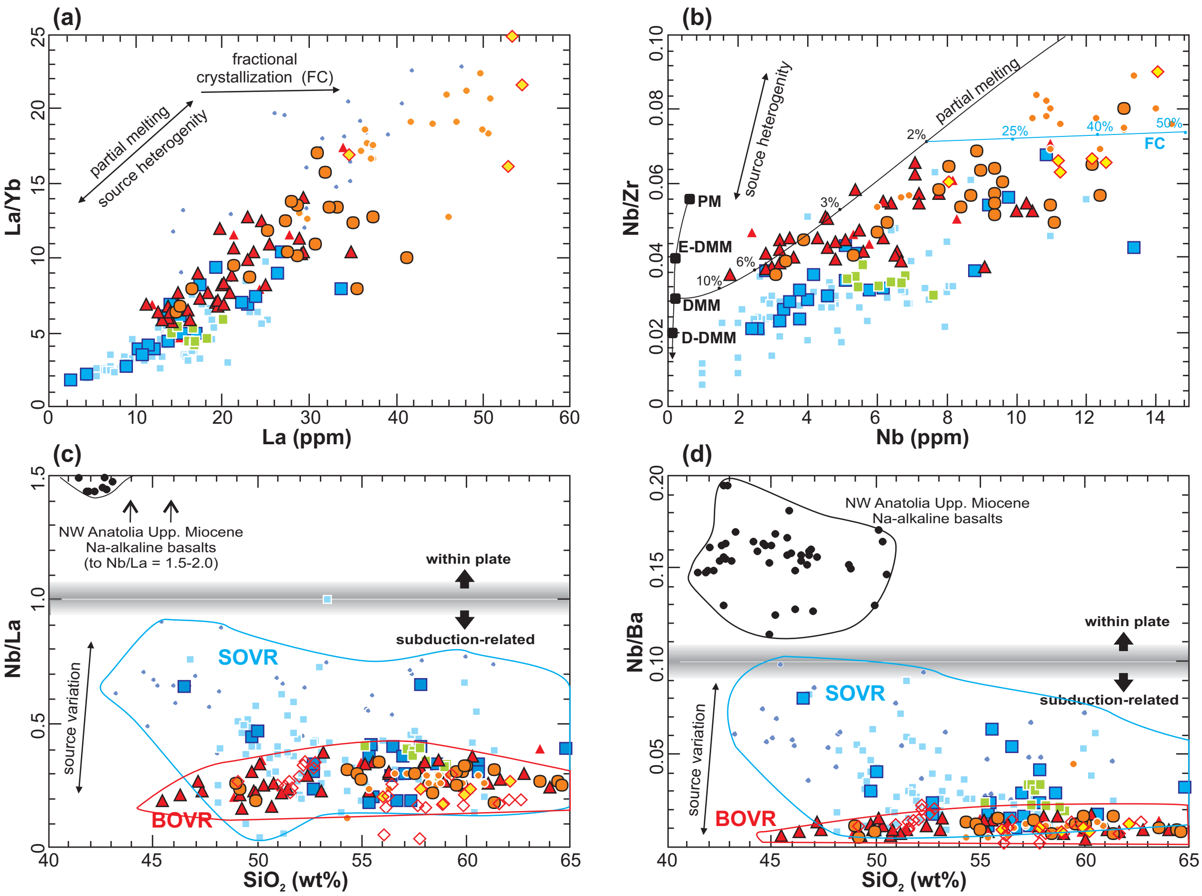

Figure 12. Whole-rock (a) La/Yb versus La (ppm), (b) Nb/Zr versus Nb (ppm), (c) Nb/La versus SiO2 (wt%) and (d) Nb/Ba versus SiO2 (wt%) plots of the studied rock groups. See Figure 6 for symbols. Also shown are the possible mantle compositions of Primitive Mantle (PM; Palme and O'Neil, 2004), Depleted MORB mantle (DMM), depleted-DMM (D-DMM), Enriched-DMM (E-DMM; Workmann and Hart, 2005). Non-modal closed system dynamic melting trend for the Depleted MORB mantle (DMM), and fractional crystallization trend (FC) of the obtained 2% partial melt is also shown on (b). Melting model uses 1% critical porosity for melt segregation and spinel-facies mantle mineralogy of ol0.53(-0.06) + opx0.27(0.28) + cpx0.17(0.67) + sp0.03(0.11) (Kinzler, 1997), where the numbers indicate mineral (and melt) modes. The partition coefficients are from Adam and Green (2006).

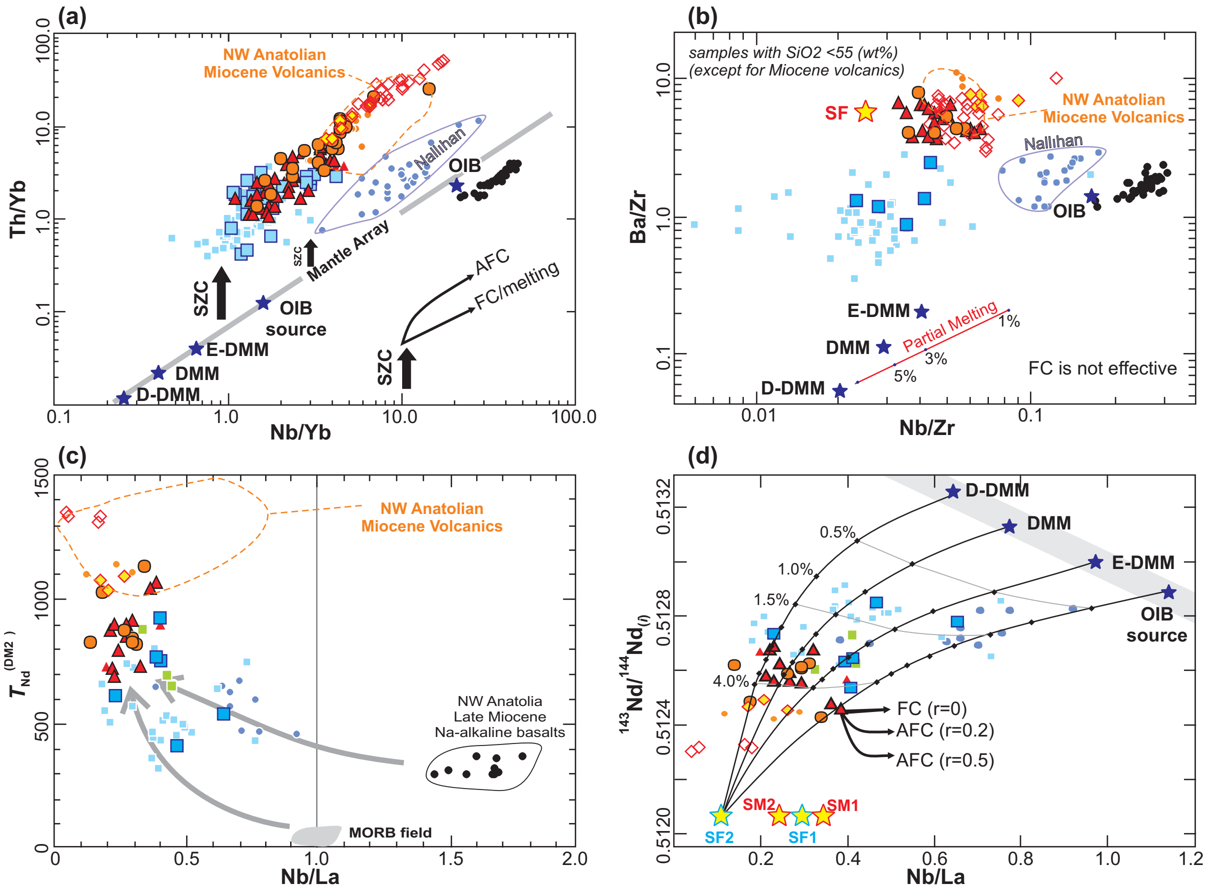

Figure 13. Whole-rock (a) Th/Yb versus Nb/Yb (Pearce, 2008), (b) Ba/Zr versus Nb/Zr, (c) TDMM(2) versus Nb/La and (d) 143Nd/144Nd(I) versus Nb/La plots of the studied rock groups. Depleted MORB mantle (DMM), depleted-DMM (D-DMM), Enriched-DMM (E-DMM; Workmann and Hart, 2005), average OIB compositions (Workmann et al., 2004) and OIB source (Norman and Garcia, 1999) are also shown to mark the mantle compositional array on (a), (b) and (d). Non-modal dynamic melting model is also shown on (b) by using D-DMM source composition with spinel-facies mantle mineralogy (Kinzler, 1997) and 1% critical porosity for melt segregation. Second-stage Nd DMM model ages on (c) are calculated according to Keto and Jacobsen (1987). Subduction Fluid (SF) and Subduction Melt (SM) compositions on (d) are calculated by using fluid and melt partition coefficients of Johnson and Plank (1999) and the procedures given in Münker (2000). See Table 3 for calculated compositions of SF1, SF2, SM1 and SM2. Simple mixing curves between SF2 and distinct mantle sources are also shown on (d). FC and AFC vectors are calculated for 90% crystallization of a mineral assemblage of olivine0.30+clinopyroxene0.30+plagioclase0.40 from a melt represented by the sample C-15. AFC vectors are calculated for r=0.2 and r=0.5 (relative ratio of assimilated material to crystallized material) Composition of assimilating material for the AFC model on (d) is: Nb=12 ppm; La= 40 ppm; 143Nd/144Nd=0.5120. See text for details and to Figure 6 for symbols.

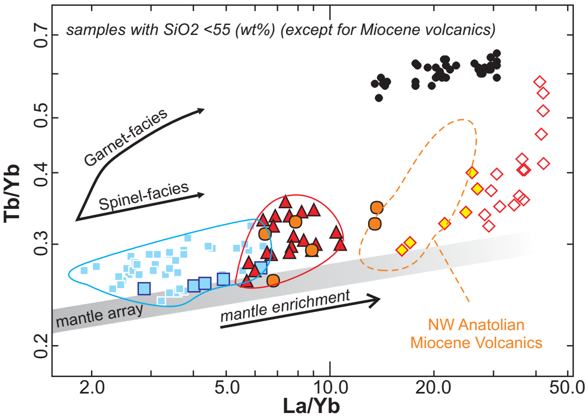

Figure 14. Tb/Yb vs La/Yb systematics of the studied rock groups. Approximate curves for partial melts from garnet- and spinel-bearing mantle are also shown. See text for details and to Figure 6 for symbols.